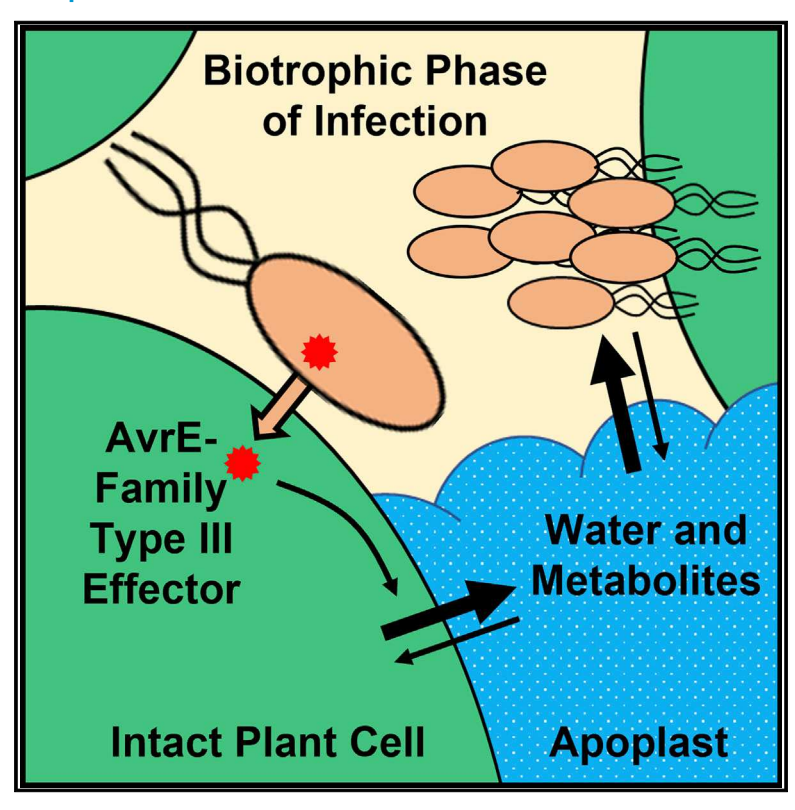
Dynamic nutrient acquisition from a hydrated apoplast supports biotrophic proliferation of a bacterial pathogen of maize

Graphical abstract



Authors

Irene Gentzel, Laura Giese, Gayani Ekanayake, ..., Jean-Christophe Cocuron, Ana Paula Alonso, David Mackey

Correspondence

mackey.86@osu.edu

In brief

Phyotpathogenic bacteria acquire water and host metabolites from the apoplast, but the extent of their mobilization during biotrophy is unknown. Gentzel et al. demonstrate that a type III effector from a widely distributed family promotes dynamic nutrient acquisition from a hydrated apoplast prior to the disruption of plant-cell integrity.

Highlights

- A bacterial pathogen of maize causes apoplast hydration during biotrophy
- The hydrated apoplast becomes enriched in metabolites utilizable by the bacteria
- Metabolite accumulation in and bacterial assimilation from the apoplast are dynamic
- An effector from a widely distributed family drives water and nutrient availability







Article

Dynamic nutrient acquisition from a hydrated apoplast supports biotrophic proliferation of a bacterial pathogen of maize

Irene Gentzel, 1,2,3 Laura Giese, 2 Gayani Ekanayake, 2 Kelly Mikhail, 2 Wanying Zhao, 2 Jean-Christophe Cocuron, 4 Ana Paula Alonso, 4,5,6 and David Mackey 2,7,8,9,*

- ¹Translational Plant Sciences Graduate program, The Ohio State University, Columbus, OH 43210, USA
- ²Department of Horticulture and Crop Science, The Ohio State University, Columbus, OH 43210, USA
- ³Department of Plant Pathology, The Ohio State University, Columbus, OH 43210, USA
- ⁴BioAnalytical Facility, University of North Texas, Denton, TX 76203, USA
- ⁵BioDiscovery Institute, University of North Texas, Denton, TX 76203, USA
- ⁶Department of Biological Sciences, University of North Texas, Denton, TX 76203, USA
- ⁷Department of Molecular Genetics, The Ohio State University, Columbus, OH 43210, USA
- ⁸Center for Applied Plant Sciences, The Ohio State University, Columbus, OH 43210, USA
- ⁹Lead contact
- *Correspondence: mackey.86@osu.edu https://doi.org/10.1016/j.chom.2022.03.017

SUMMARY

Plant pathogens perturb their hosts to create environments suitable for their proliferation, including the suppression of immunity and promotion of water and nutrient availability. Although necrotrophs obtain water and nutrients by disrupting host-cell integrity, it is unknown whether hemibiotrophs, such as the bacterial pathogen *Pantoea stewartii* subsp. *stewartii* (*Pnss*), actively liberate water and nutrients during the early, biotrophic phase of infection. Here, we show that water and metabolite accumulation in the apoplast of *Pnss*-infected maize leaves precedes the disruption of host-cell integrity. Nutrient acquisition during this biotrophic phase is a dynamic process; the partitioning of metabolites into the apoplast rate limiting for their assimilation by proliferating *Pnss* cells. The formation of a hydrated and nutritive apoplast is driven by an AvrE-family type III effector, WtsE. Given the broad distribution of AvrE-family effectors, this work highlights the importance of actively acquiring water and nutrients for the proliferation of phytopathogenic bacteria during biotrophy.

INTRODUCTION

The need of phytopathogens to suppress host immunity is well established (Jones and Dangl, 2006). More recently, the importance of nutritional susceptibility, including increased water and nutrient availability at the site of pathogen proliferation, is emerging (El Kasmi et al., 2018). Notably, the distinction between defense suppression and nutritional susceptibility is somewhat ambiguous. For example, pattern-triggered immunity (PTI), which is induced upon recognition of microbe- or self-derived elicitors, activates transporters that reduce the availability of apoplastic sugar (Naseem et al., 2017; Yamada et al., 2016). Thus, the suppression of PTI may promote nutritional susceptibility by preventing a decrease of apoplastic sugar availability. Bacteria deploy type III secretion systems to translocate type III effectors (T3Es) into nearby host cells (Wagner et al., 2018). T3Es of the transcriptional activator-like (TAL) family from Xanthomonas induce the transcription of SWEET-family sugar exporters, but whether this overcomes defense-induced sugar deprivation or promotes additional nutrient availability is unknown (Chen et al., 2010). The presence of resistance genes that use "decoy" promoter elements to redirect TAL effectors to the promoters of defense executor genes may further indicate the overlap between the control of nutritional susceptibility and host defense. Similarly, inter-related roles are apparent for apoplastic amino acid (AA) accumulation in providing nutrients, signals that promote pathogen virulence, and signals that induce plant defense responses (Sonawala et al., 2018).

Water availability also plays a central role in susceptibility and host immune defense. Water soaking (WS), which is the macroscopic hydration of the apoplast, is a symptom associated with many plant diseases and also triggers the proliferation of typically non-pathogenic endophytic bacteria (Aung et al., 2018; Xin et al., 2016). Conversely, reduced apoplast hydration following the activation of host immunity contributes to the restriction of bacterial growth (Freeman and Beattie, 2009). A TAL effector from X. gardneri, AvrHah1, promotes WS dependent on its ability to activate the expression of a secreted pectate lyase (Schwartz et al., 2017). Metabolites released by the pectate lyase may link nutrient availability and apoplast hydration by serving as both C sources and solute that decreases apoplast water potential, as has been noted during the susceptible interaction of Pseudomonas syringae with Arabidopsis (Wright and Beattie, 2004). TAL effectors that induce transporters promoting apoplastic sugar accumulation also induce WS, further pointing to a link between these aspects of nutritional susceptibility.



Article



However, how nutritional susceptibility is induced by the preponderance of plant pathogenic bacteria that lack TAL effectors is poorly understood.

AvrE-family T3Es are broadly distributed among and make key contributions to the virulence of multiple genera of TAL-deficient plant pathogenic bacteria, including Pantoea, Pseudomonas, Erwinia, Ralstonia, and Pectobacteria. The ability of AvrE-family T3Es to promote the virulence of these diverse bacteria likely results from their multi-functionality, which includes the suppression of host defense, induction of WS, and promotion of diseaseassociated necrosis (Frederick et al., 2001; Gaudriault et al., 1997; Kim et al., 2011; Mor et al., 2001). Pantoea stewartii subsp. stewartii (Pnss) colonizes both the xylem and apoplast of maize leaves where it causes Stewart's wilt and leaf blight, respectively (Pataky, 2003; Roper, 2011). Unlike the typically modest contribution of individual T3Es to bacterial virulence, perhaps resulting from dispensability or functional redundancy (Kvitko et al., 2009), WtsE is essential to the virulence of Pnss. Mutations that disrupt either the type III secretion system or just WtsE cause similar and dramatic reductions in the ability of Pnss to proliferate, induce WS, and cause disease-associated necrosis in the apoplast of infected maize leaves (Ham et al., 2006). Thus, the Pnss-maize interaction is an excellent model for examining the role of a single T3E in the bacterial acquisition of water and nutrients from a host plant. Furthermore, the hemibiotrophic lifestyle of *Pnss* on maize, characterized by its proliferation in living and, later, dying or dead host tissue, makes the system suitable for addressing a major knowledge gap about the relationship between host-cell integrity and nutritional susceptibility.

We show here that Pnss promotes nutritional susceptibility within the apoplast of maize leaves during the biotrophic phase of infection. WtsE-dependent apoplast hydration preceded both macroscopic WS and disruption of host-cell integrity. WtsE also induced the accumulation of specific metabolites in the apoplast without altering their total levels in the leaf and prior to disrupting the integrity of the maize cells. The amount of Pnssassimilated carbon (C) and nitrogen (N) indicated that the arrival of metabolites into the apoplast dynamically supports Pnss proliferation during the biotrophic phase of infection. Consistent with this conclusion, the delivery of WtsE into maize cells by a heterologous, non-proliferating delivery system induced rapid apoplast hydration and the accumulation of substantially higher levels of metabolites in the apoplast. Additionally, the metabolites that WtsE caused to over-accumulate in the absence of assimilation match those that supported Pnss growth as sole sources of C or N. Thus, Pnss promotes nutritional susceptibility during the biotrophic phase of infection by deploying WtsE to establish an aqueous and dynamically nutritive apoplast.

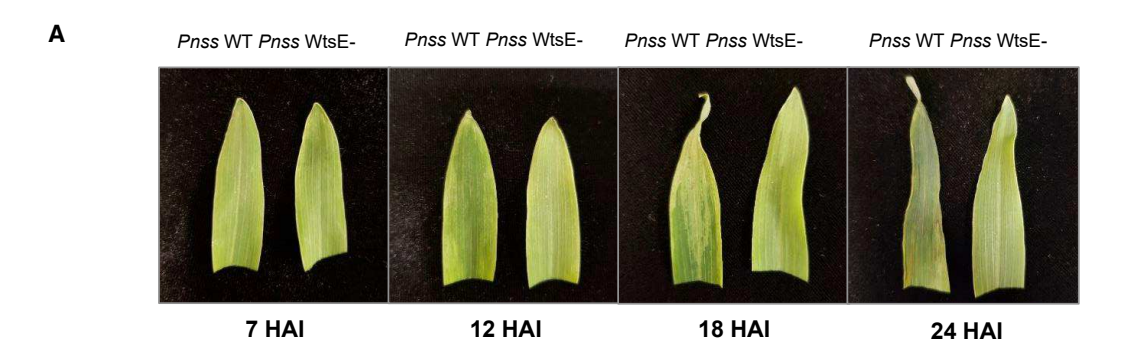
RESULTS

Pnss induces water soaking during the biotrophic phase of infection

Pnss infection of the apoplast of maize leaves causes WS followed by necrosis (Ham et al., 2006). Whether WS precedes or results from the early stages of necrosis is of fundamental importance for understanding the physiology of disease progression. Although the symptoms associated with natural infections progress asynchronously within and in advance of growing disease lesions, vacuum infiltration of a high titer of Pnss into the apoplast of maize leaves synchronizes the events of disease progression at the scale of whole leaves. The first true leaf of maize seedlings infected with wild-type Pnss (Pnss WT) or a non-polar wtsE mutant strain (Pnss WtsE-) revealed WtsE-dependent WS by 12 h after infiltration (HAI) that transitioned to increasingly severe necrosis by 18 and 24 HAI (Figure 1A). Measuring apoplast hydration (Gentzel et al., 2019) revealed progression toward WS in advance of macroscopic symptoms (Figure 1B). The apoplast was flooded to \sim 85% capacity at 0 HAI, and the level of hydration decreased to <50% by 3 HAI regardless of inoculum type. In plants infiltrated with buffer or Pnss WtsE-, apoplast hydration continued to decrease steadily, nearly reaching the $\sim 15\%$ level observed in untouched plants by 12 HAI. Notably, the apoplast hydration of plants infiltrated with Pnss WT increased following 3 HAI and differed significantly from Pnss WtsE- by 7 HAI. By 12 HAI, when macroscopic symptoms were first apparent, apoplast hydration in the leaves infiltrated with Pnss WT had risen to nearly 70%. Consistent with a positive relationship between apoplast hydration and bacterial growth, the abundance of Pnss WT, in a well-hydrated apoplast, increased by ~100-fold between 7 and 24 HAI, whereas Pnss WtsE-, in a drying apoplast, scarcely proliferated beyond 7 HAI (Figure 1C).

With this more precise knowledge of the timing of WS, we next sought to determine the relationship between WS and necrosis. First, we indirectly assessed host-cell integrity by measuring ion leakage (Figure 2A). Notably, despite the significant increase in apoplast hydration induced by Pnss WT at 7 HAI, conductivity of the leaf bath solution at this time did not differ between untouched plants and those infiltrated with buffer, Pnss WtsE-, and Pnss WT. WtsE-dependent increases in conductivity, which were modest at 12 HAI and strong at 24 HAI, coincided with the earliest macroscopic WS at 12 HAI and severe necrosis at 24 HAI. Given that the infiltration with Pnss WtsE-, which caused no macroscopic symptoms (Figure 1A), induced conductivity at 24 HAI comparable with that induced by Pnss WT at 12 HAI, it is unclear whether the modest conductivity induced by Pnss WT at 12 HAI resulted from the disruption of host cells. To directly assess cellular integrity, propidium iodide (PI)-stained leaves were examined by confocal microscopy. PI stains cell walls and, when not excluded by an intact plasma membrane, nuclear DNA and other intracellular structures (Jones et al., 2016). In untouched plants, PI stained epidermal and mesophyll cell walls, with low levels of intracellular staining (Figure 2B). Maize seedlings infiltrated with 5% DMSO as a positive control for damaged plasma membranes (Gentzel et al., 2019) displayed a loss of cell wall definition and extensive intracellular staining of both epidermal and mesophyll cells. The leaves infiltrated with Pnss WtsE- did not differ from the untouched leaves at either 12 or 18 HAI. The leaves infiltrated with Pnss WT were also similar to the untouched leaves at 12 HAI but displayed disorganization of cell walls and intracellular staining in both epidermal and mesophyll cells by 18 HAI. Quantification of intracellular PI staining in the leaves that were untouched or infiltrated with Pnss WT or Pnss WtsE- confirmed these patterns (Figure 2C). Thus, the disruption of the plasma membrane of maize cells likely accounts for the development of necrotic symptoms by 18 HAI (Figure 1A) and the increase in conductivity observed at 24 HAI (Figure 2A).





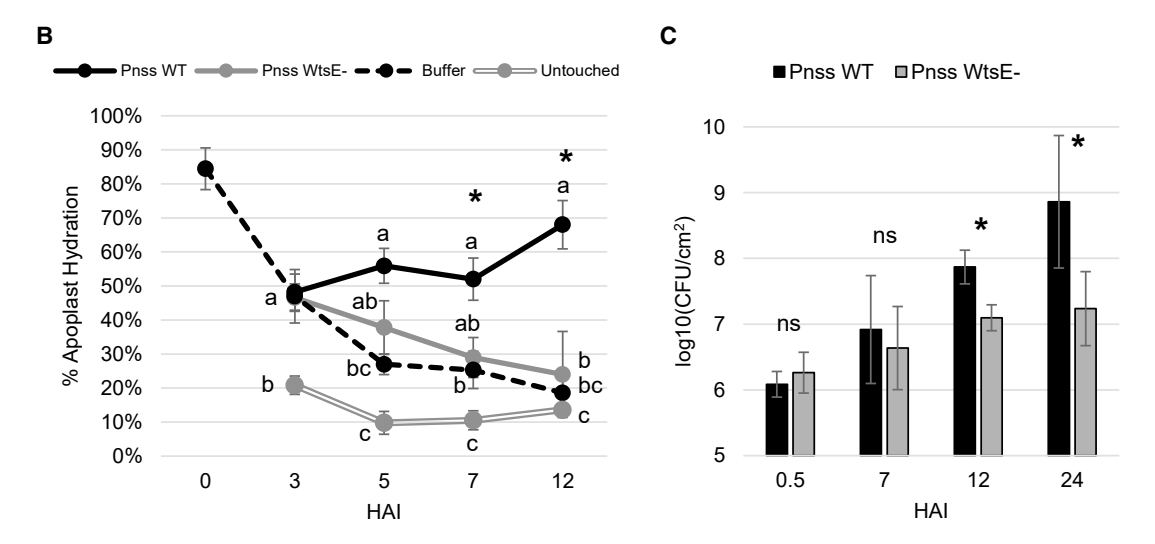


Figure 1. Apoplast hydration coincides with the proliferation of Pnss in maize leaves

(A) First true leaves of maize at the indicated times after infiltration with Pnss WT or Pnss WtsE-.

(B) Apoplast hydration following the infiltration of maize leaves with Pnss WT, Pnss WtsE-, or buffer and in untouched plants with standard error. Six to eight leaves were assessed individually at each time point within each of three biological replicates. Different letters indicate significance between treatments at each time point calculated with ANOVA followed by Tukey's HSD test where p < 0.05. Asterisks (*) indicate significance differences between Pnss WT and Pnss WtsE- as assessed with Student's t test where p < 0.05.

(C) Growth of Pnss following vacuum infiltration into the first true leaves of maize with standard error. The data represent three biological replicates with standard error for n = 9 for each treatment/time point. Asterisks indicate significance differences at the indicated time as assessed with Student's t test where p < 0.05 and ns = not significant.

Collectively, these data indicate that WS during *Pnss* infection is not driven by the release of apoplastic contents from disrupted host cells. Rather, *Pnss* induces apoplast hydration and proliferates during the biotrophic phase of infection.

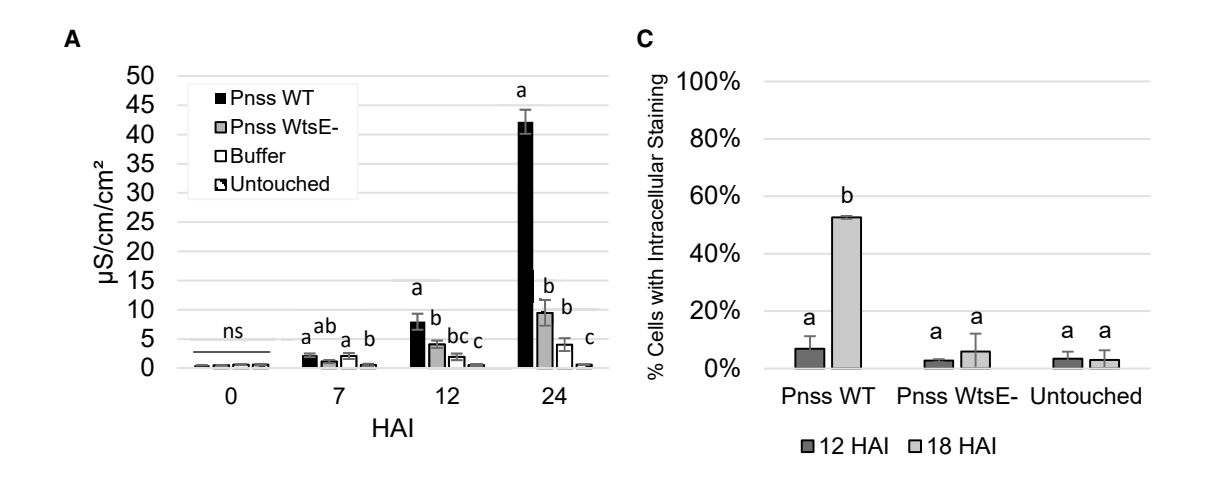
Pnss induces the accumulation of metabolites in the hydrated apoplast

Beyond the correlation with increased water availability, we speculated that additional, WtsE-dependent modifications of the apoplast contribute to the growth of *Pnss* during the biotrophic phase of infection. One possibility is the suppression of host defense responses, a known activity of WtsE and other AvrE-family T3Es (Degrave et al., 2015). Here, we tested the non-exclusive hypothesis that WtsE promotes nutritional susceptibility by increasing the availability of metabolites within the hydrated apoplast. Quantification of AAs (27 analyzed), sugars (18 analyzed), organic acids (OAs, 23 analyzed), phosphorylated

compounds (PCs, 54 analyzed), and phenolic compounds (19 analyzed) in the apoplast fluid isolated from the first true leaves of maize seedlings, as well as the residual leaf tissue, allowed the determination of the abundance of these metabolite classes in the whole leaf (Figures 3A and 3B) and the apoplast (Figures 3C and 3D), as well as the their partitioning between the intact cellular and apoplast compartments (Figures 3E and 3F). Notably, cytosolic contamination of apoplast preparations was minimal, as indicated by the presence of less than 0.3% of PCs in the apoplast of the untouched leaves at 7 HAI (Figure 3E).

We first considered how flooding of the apoplast, as it occurs during vacuum infiltration-mediated infection, affects metabolite abundance and partitioning. Whole leaves at 7 HAI with buffer, relative to the untouched leaves, did not differ in the overall abundance of any of the metabolite classes (Figure 3A) but did display increased levels and partitioning of water-soluble metabolites into the apoplast (Figures 3C and 3E). This phenomenon, which





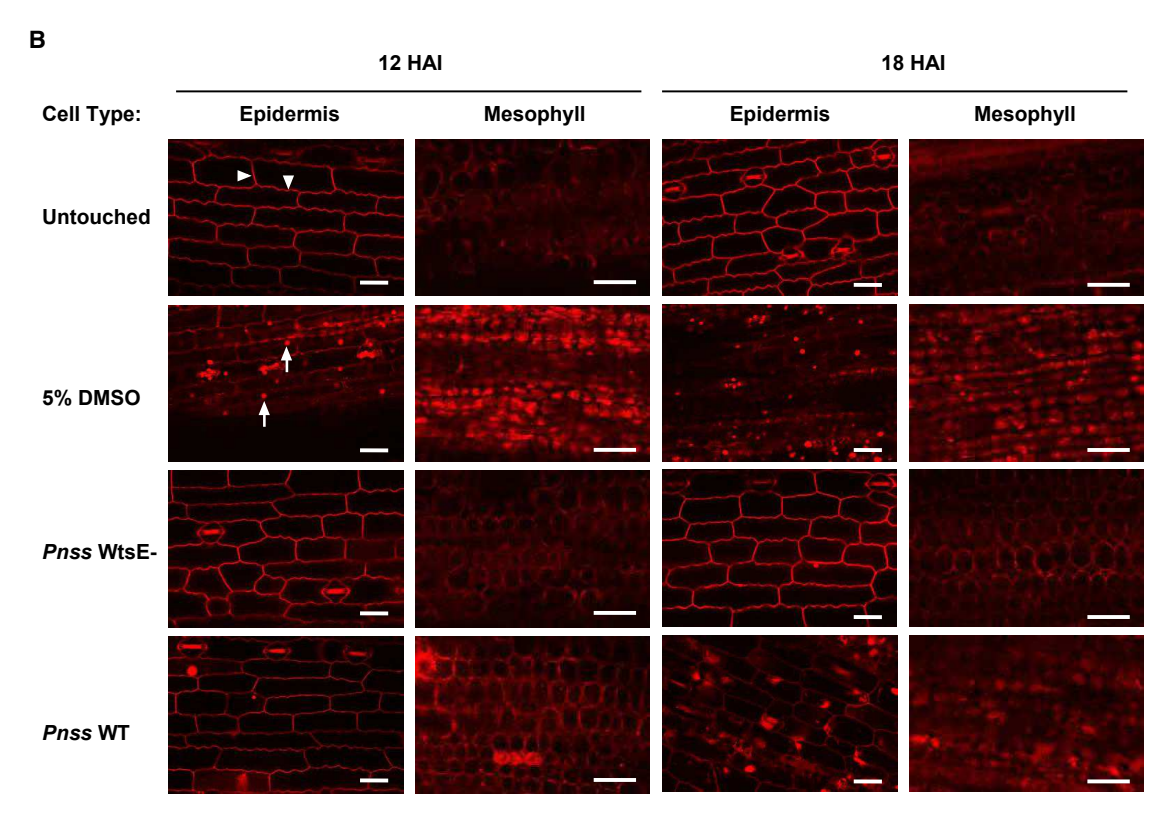


Figure 2. Timing of disruption of host-cell integrity by Pnss

(A) Ion leakage measurements of maize leaves following the infiltration with Pnss WT, Pnss WtsE-, or buffer and in untouched plants with standard error. Data are from 4 biological replicates, each consisting of 2 technical replicates (n = 8). Different letters indicate significance via ANOVA and Tukey's HSD test where p < 0.05.

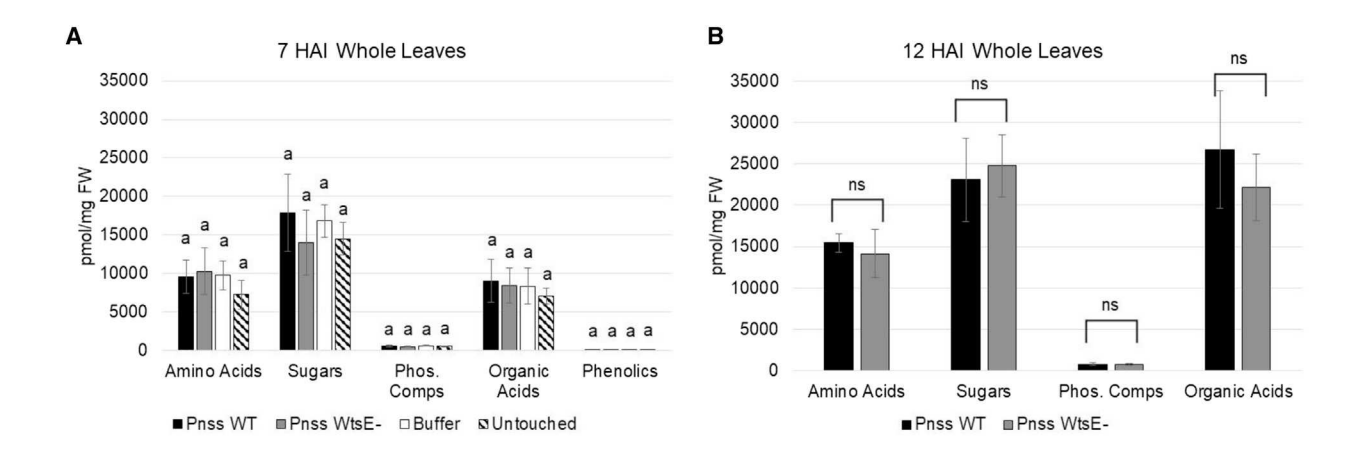
(B) Confocal microscopy images of propidium iodide (PI)-stained maize epidermal and mesophyll cells at 12 and 18 HAI with Pnss WT, Pnss WtsE-, 5% DMSO, or untouched plants. PI stains cell walls (arrowheads) as well as intracellular structures (arrows) of cells with permeable plasma membranes. Images are from one biological replicate and are representative of three biological replicates. Scale bars, 100 μm.

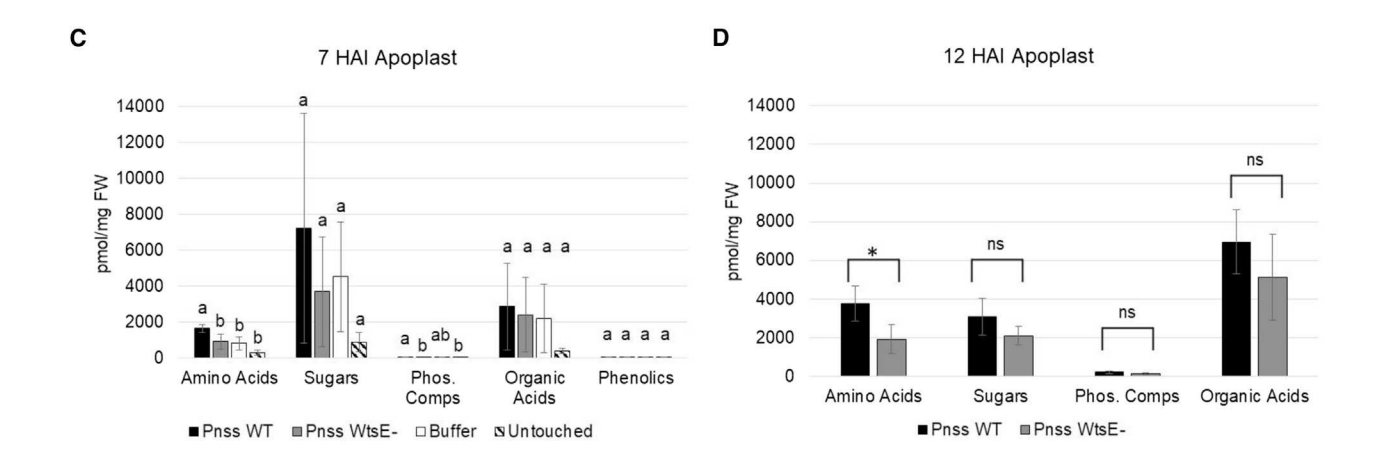
(C) Quantification of intracellular PI staining in the epidermal cells of the leaves infiltrated with Pnss WT or Pnss WtsE- and untouched plants. Data are from three biological replicates and error bars are standard deviation between replicates. The number of cells counted for Pnss WT, Pnss WtsE-, and untouched were 982, 916, and 985 at 12 HAI and 578, 483, and 500 at 18 HAI, respectively. Different letters indicate statistical significance assessed by ANOVA and Tukey's HSD test across all treatments and time points where p < 0.05.

will be referred to as the "buffer effect," may increase nutrient accessibility and thus contribute to the modest proliferation of both Pnss WT and Pnss WtsE—during the first 7 HAI (Figure 1C). We also considered the influence of plant defense, specifically

PTI that likely occurs in response to Pnss WtsE-, on metabolite abundance and partitioning. Leaves infiltrated with Pnss WtsEor buffer did not differ for any metabolite class in total abundance, apoplast abundance, or partitioning into the apoplast







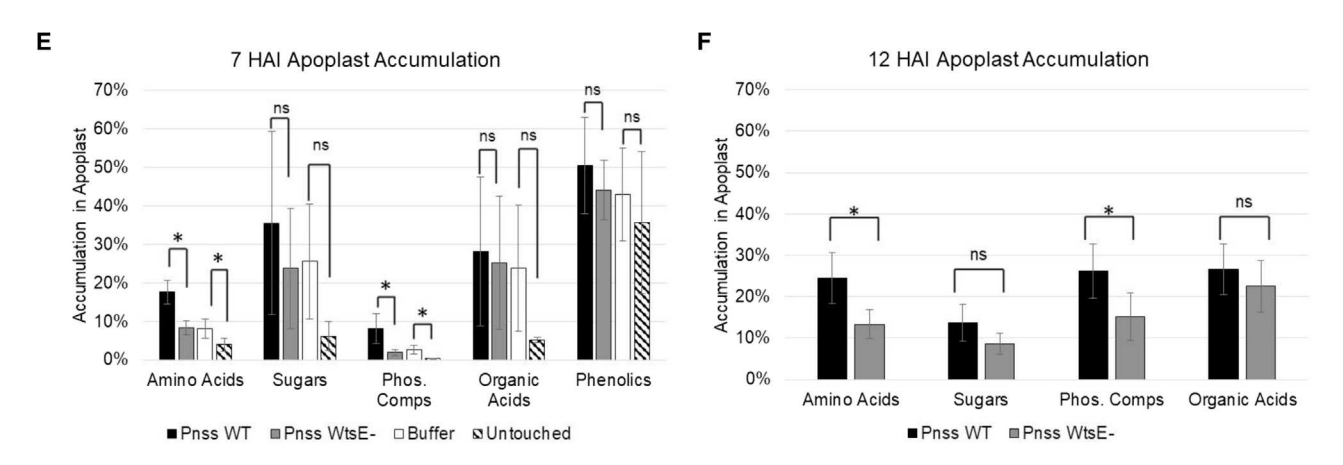


Figure 3. Abundance and partitioning into the apoplast of metabolite classes during Pnss infection

Maize plants were infiltrated with Pnss WT, Pnss WtsE-, or buffer or were left untouched, and the metabolite composition of the apoplast fluids and remaining leaves after apoplast removal were assessed.

(A and B) Abundance of the indicated metabolite classes in the whole leaves at 7 and 12 HAI, respectively.

(C and D) Abundance in the apoplast at 7 and 12 HAI, respectively.

(E and F) Percentage of each metabolite class from the whole leaves that are present in the apoplast. Error bars are standard deviation from four biological replicates, each comprising one technical replicate (n = 4). Letters represent significance assessed by ANOVA followed by Tukey's HSD test where p < 0.05. Asterisks indicate significant differences as assessed by Student's t test where p < 0.05 and ns = not significant.



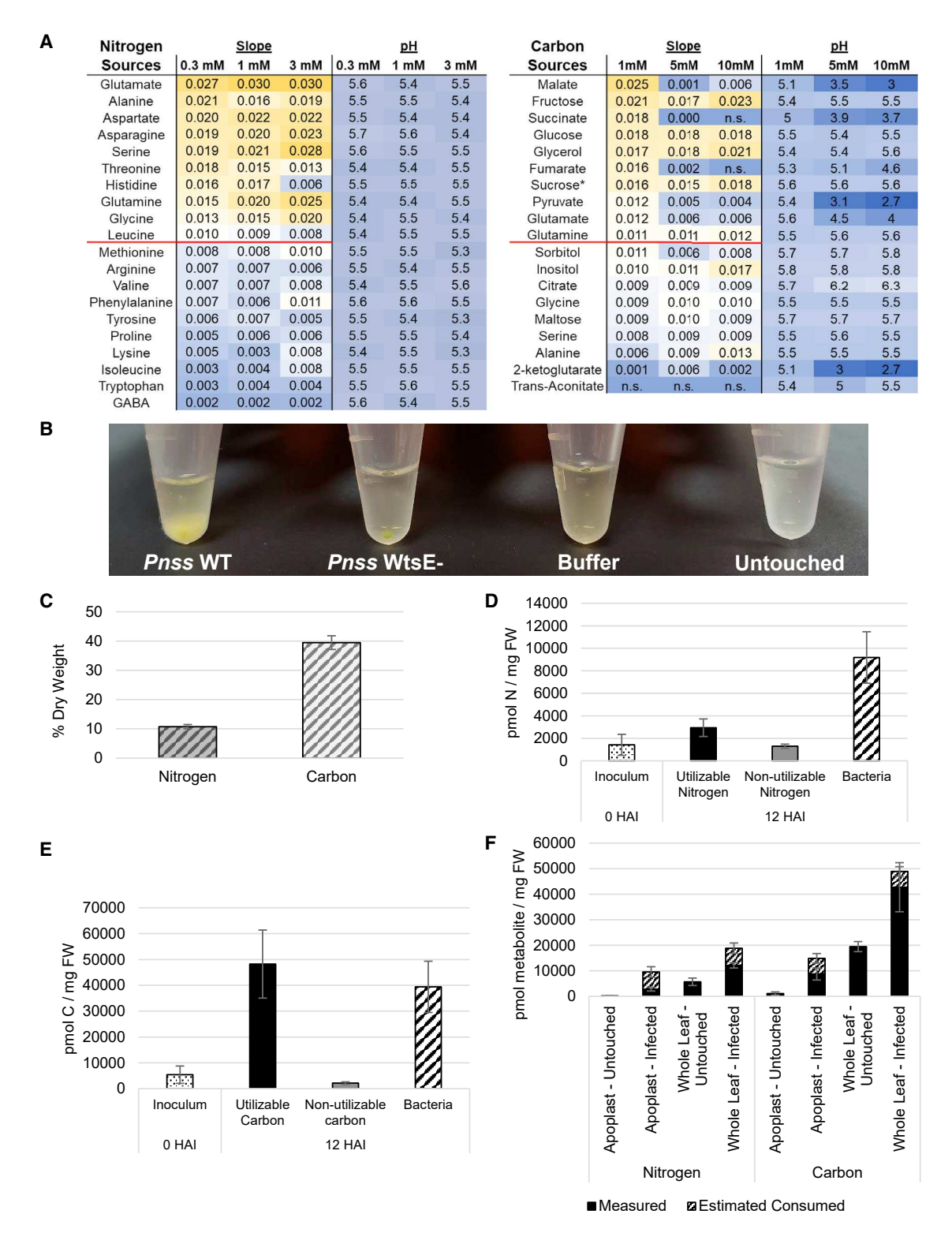


Figure 4. Utilization and consumption of N and C sources in the maize apoplast by Pnss

(A) Heatmap of slopes of Pnss WT growth curves between 4 and 8 h in minimal media containing the indicated concentrations of sole sources of N (left) or C (right) and additional heatmap of the pH of the individual growth media. Metabolites with slopes greater than $1.5 \times$ that of the negative controls (no N = 0.0061 and no C = 0.0075) were considered efficiently utilized (above red lines). Asterisk indicates that the concentrations of sucrose were evaluated at 0.5, 2.5, and 5 mM. Slope data are the average of \geq 6 technical replicates for each metabolite at each concentration. n.s. indicates negative slope.

(B) Bacteria pellet sizes in apoplast fluid recovered at 12 HAI with Pnss WT or Pnss WtsE— and compared with the lack of pellet in buffer-infiltrated and untouched controls.



Cell Host & Microbe Article

(Figures 3A–3C). Furthermore, for no individual metabolite did the apoplast abundance differ at 7 HAI with *Pnss* WtsE– versus buffer (Figure S1). Thus, assuming *Pnss* WtsE– triggers PTI, effects of PTI on the accumulation of the surveyed metabolites in the apoplast are either absent or are masked by the "buffer effect."

Most significantly, we determined whether infection with Pnss WT influences metabolite abundance and partitioning in infected maize leaves. Whole leaf abundance did not differ for any metabolite class between Pnss WT and any of the other treatments at either 7 or 12 HAI (Figures 3A and 3B). However, significant increases in the abundance and partitioning of AAs and PCs in the apoplast of maize leaves were apparent at both 7 and 12 HAI with *Pnss* WT, relative to *Pnss* WtsE- (Figures 3C-3F). Notably, the increased accumulation of metabolites in the apoplast following infection with Pnss WT, relative to Pnss WtsE-, is in addition to increases from the "buffer effect." Significant increases in apoplast accumulation, which is dependent on WtsE, were apparent at both 7 and 12 HAI for many individual AAs but for none of the much less abundant PCs (Figures S1 and S2). WtsE did not increase apoplast accumulation or partitioning of sugars or OAs as metabolite classes at either time point (Figures 3C-3F). Differences in metabolite abundance in the apoplast do not result from differences in bacterial abundance. At 7 HAI, apoplast levels of AAs and PCs differ despite the growth of *Pnss* WT and *Pnss* WtsE— to similar levels (Figure 1C). At 12 HAI, elevated levels of AAs and PCs persist in the apoplast of the plants infected with Pnss WT, relative to Pnss WtsE-, despite the likely opposing contribution of nutrient assimilation by the more abundant Pnss WT. Also, further linking the function of WtsE to the apoplastic accumulation of AAs and PCs, an inactive derivative with mutations to each of two WxxxE motifs (Figures S3A and S3B; Ham et al., 2009) failed to alter apoplast or whole leaf accumulation of any class of metabolites, relative to a Pnss WtsE- (Figures S3C and S3D).

Additional analyses support the conclusion that WtsE does not cause metabolites to accumulate in the apoplast by causing leakage from disrupted host cells. First, the difference in the profile of AAs in the apoplast at 12 HAI with *Pnss* WT versus 5% DMSO indicates that *Pnss* infection alters metabolite availability in the apoplast distinctly from that observed following membrane disruption (Figure S4A). Also, malate dehydrogenase (MDH) activity was measured in the apoplast and residual leaf samples from the untouched leaves and leaves at 7 and 12 HAI with buffer, *Pnss* WtsE—, or *Pnss* WT (Figure S4B). Consistent with maize cells retaining their integrity in each of these samples, all had less than 0.1% of the total MDH activity in the apoplast. Remarkably, apoplast from the leaves at 12 HAI with 5% DMSO also contained less than 0.1% of total MDH activity, indi-

cating that PI staining detects disruptions to cellular integrity (Figure 2B) that do not cause accumulation of MDH in the apoplast. Thus, dependent on WtsE, *Pnss* causes AAs and PCs to accumulate in the apoplast of infected maize leaves prior to the loss of plant-cell integrity.

We next considered the source of metabolites accumulating in the space outside of intact plant cells. One hypothesis is that WtsE perturbs the partitioning of metabolites between intact leaf cells and the apoplast, which is supported by the observation that WtsE interacts with plasma membrane-localized phosphatases and kinases in these local cells (Jin et al., 2016). An alternative hypothesis is that WtsE causes the mobilization of metabolites to the leaf apoplast from a systemic source, which is supported by the continued mobilization of protein from the seed store in the 6- to 7-day-old seedlings used for these experiments (Figure S5A). To distinguish between these possibilities, we established a detached leaf assay in which Pnss causes WtsE-dependent WS that is progressing to necrosis by 24 HAI (Figure S5B). At 12 HAI with buffer, Pnss WtsE-, or Pnss WT, prior to symptom development, the whole leaf abundance of AAs did not differ (Figure S5C). However, relative to buffer or Pnss WtsE-, Pnss WT caused significant increases in the abundance and partitioning of AAs in the apoplast (Figure S5C) Similar to intact plants, WtsE caused many individual AAs to accumulate significantly in the apoplast despite having little effect on their overall abundance (Figures S5D and S5E). Thus, the abundance of AAs in the apoplast increases during the biotrophic phase of Pnss infection because WtsE alters their partitioning between local, intact plant cells and the apoplast.

Dynamic accumulation of host metabolites in and their assimilation from the apoplast supports *Pnss* growth

An extension of the hypothesis that Pnss promotes nutritional susceptibility by increasing metabolite abundance in the apoplast is that the accumulating metabolites are utilizable as bacterial nutrients. Thus, individual metabolites that accumulate in the apoplast of infected plants were tested for their ability to support Pnss growth as sole sources of N or C. For sources of N, we tested 20 AAs, including GABA and all the proteinogenic AAs except cysteine, which comprise >99% of the total AAs in the apoplast at 12 HAI with Pnss WT. For sources of C, we tested 7 sugars, including the 5 most abundant; the 7 most abundant OAs; and 5 AAs, including the 4 most abundant, which comprise 98%, 97%, and 69% of the total sugars, OAs and AAs, in the apoplast at 12 HAI with Pnss WT, respectively. Individual metabolites were ranked based on the growth rate they supported (Figure 4A). Those that most efficiently support Pnss growth are abundant in the apoplast of the maize leaves infected with Pnss WT (Figure S2). For example, the 7 best utilized C sources,

⁽C) Abundance of N and C within Pnss WT recovered in apoplast at 12 HAI.

⁽D) Apoplast amino acids segregated as utilizable (above the red line in A) or non-utilizable and represented as pmol N per mg FW. Also shown are amounts of N in *Pnss* inoculated at time 0 and isolated with apoplast fluid at 12 HAI.

⁽E) Similar to (D), but representing C from utilizable and non-utilizable metabolites. Data in (D) and (E) for inoculum and apoplast bacteria are from one biological replicate consisting of three pools of four extracts each, and error bars are standard deviation. Apoplast metabolite quantities are calculated from the data in Figures S1 and S2.

⁽F) Quantities of utilizable N or C sources in apoplast or whole leaves of untouched plants at 7 HAI compared with apoplast or whole leaves at 12 HAI with Pnss WT (black bars). The estimated quantity of metabolites consumed as sources of N or C by Pnss during its growth in planta by 12 HAI is indicated with hashed bars (see text for explanation of estimates). Error bars are standard deviation.

Article



malate, fructose, succinate, glucose, glycerol, fumarate, and sucrose, comprise the 4 most abundant sugars and 3 of the 5 most abundant OAs in the apoplast at 12 HAI with Pnss WT. Similarly, the 3 most abundant AAs in the apoplast, Glu, Ala, and Ser, are 3 of the 5 best utilized N sources. Thus, Pnss is physiologically well tuned to efficiently utilize the N and C sources abundant in its apoplast niche.

The observation that metabolites abundant in the apoplast during Pnss infection are efficiently assimilated by the bacteria indicated a potentially dynamic relationship between their arrival into and bacterial uptake from the apoplast. Notably, the metabolite quantities measured in apoplast extracts do not include metabolites already assimilated by the bacteria, presumably biased to those abundant and most efficiently utilized by Pnss. To begin to understand the magnitude of assimilation, we used elemental analysis to measure the abundance of N and C in the Pnss isolated from maize leaves at 12 HAI (Figure 4B). As determined in the study conducted by Gentzel et al. (2019), our method for the isolation of apoplast fluid also recovers >80% of viable Pnss WT cells but <20% of Pnss WtsE-cells, possibly resulting from defense-associated cross-linking of the latter to plant cell walls (Mitchell et al., 2015). Unlike Pnss WT, the lower growth and recovery of Pnss WtsE- cells provided an insufficient sample for elemental analysis. Consistent with the C:N molar ratios of 3.32-4.01 for Pseudomonas and Erwinia spp. isolated from grassland litter and cultured in rich media (Mouginot et al., 2014), N and C constituted \sim 10% and \sim 40% of the dry weight of the Pnss WT isolated from infected maize leaves (Figure 4C). Notably, the sliminess of the Pnss WT pellet (Figure 4B) indicated the isolation of bacterially produced stewartan (Langlotz et al., 2011), an extracellular polysaccharide, although the efficiency of the isolation of this potentially significant sink for assimilated C is unknown.

We next compared the N and C assimilated by Pnss with the availability of N and C in the apoplast. Apoplast metabolites were separated into "utilizable" and "non-utilizable" categories (above or below red line in Figure 4A) and converted into picomoles of N or C per milligram fresh weight to permit direct comparison with the N and C content of Pnss WT at 0 HAI and 12 HAI (Figures 4D and 4E). Remarkably, assimilated N and C (amount in the Pnss pellet harvested at 12 HAI minus the amount in the starting inoculum at 0 HAI) were >260% and >70% of the quantity of these atoms present within the utilizable metabolites in the apoplast at 12 HAI, respectively.

The amounts of N and C assimilated by Pnss were used to estimate the pmol quantities of metabolites consumed as sources of N and C, respectively, as indicated below for N sources and based on the assumption that Pnss assimilates "utilizable" sources of N or C proportionally to their abundance in the apoplast at 12 HAI with Pnss WT.

Comparing these estimates with the abundance of "utilizable" N or C sources in the apoplast and whole leaves of untouched plants (from the 7 HAI dataset) and plants infiltrated with Pnss WT at 12 HAI indicated dynamic acquisition by Pnss (Figure 4F). By 12 HAI, Pnss had assimilated 29- and 5.5-fold more metabolites utilizable as sources of N and C, respectively, than those that were present in the apoplast of untouched plants. Notably, these are likely underestimates due to elemental analysis having been conducted on an incomplete harvest of Pnss and stewartan from the apoplast. Despite the high level of consumption, the apoplast of infected plants contained 12.4- and 7.8-fold more metabolites utilizable as N and C, respectively, than untouched plants. This ongoing availability of nutrients at and beyond 12 HAI likely contributes to the ~10-fold increase in Pnss that occurs between 12 and 24 HAI (Figure 1C).

At the level of the whole leaf, despite assimilation by Pnss of 118% and 32% of the utilizable N or C sources present in the untouched leaves, respectively, the infected leaves contained 213% and 219% as much of these metabolites as the untouched leaves. Thus, the overall levels of utilizable metabolites in infected maize leaves increased more than sufficiently to offset their dynamic flow into the apoplast and ultimately into bacterial assimilate. Collectively, these data indicate that the increased abundance of metabolites in the apoplast following infection with Pnss (Figure 3; Figures S1 and S2) represents the residual signature of a dynamic balance between their arrival into and assimilation from this infected plant compartment. Furthermore, the assimilation of AAs as sources of N is more dynamic than that for sources of C. Although secretion from Pnss may contribute to the levels of select metabolites in the apoplast, its dynamic assimilation of N and C indicates that it likely contributes little to the overall levels of apoplast metabolites.

WtsE is sufficient to convert the maize apoplast into a hydrated and nutrient-rich environment

Pnss requires WtsE to induce a hydrated and metabolite-rich apoplast and to proliferate to high levels in infected maize leaves. We hypothesized that WtsE directly promotes water and nutrient availability. Alternatively, the suppression of plant defense responses by WtsE could enable apoplast modification by other virulence factors of Pnss, such as stewartan or the RTX2 toxin (Dolph et al., 1988; Roper et al., 2015). To examine the activity of WtsE in the absence of other Pnss virulence factors, we utilized an E. coli delivery system (EcDS) comprising the Escherichia coli strain MC4100 harboring a cosmid containing the complete type III secretion system (TTSS) coding sequence from the broad host range, soft rot pathogen Dickeya dadantii (Ham et al., 1998). This strain carrying a plasmid expressing WtsE and its chaperone WtsF (EcDS-WtsE) induces disease-associated cell death in maize, which is not apparent with the control strain carrying the empty vector (EcDS-EV) (Asselin et al., 2015; Ham et al., 2006, 2008, 2009).

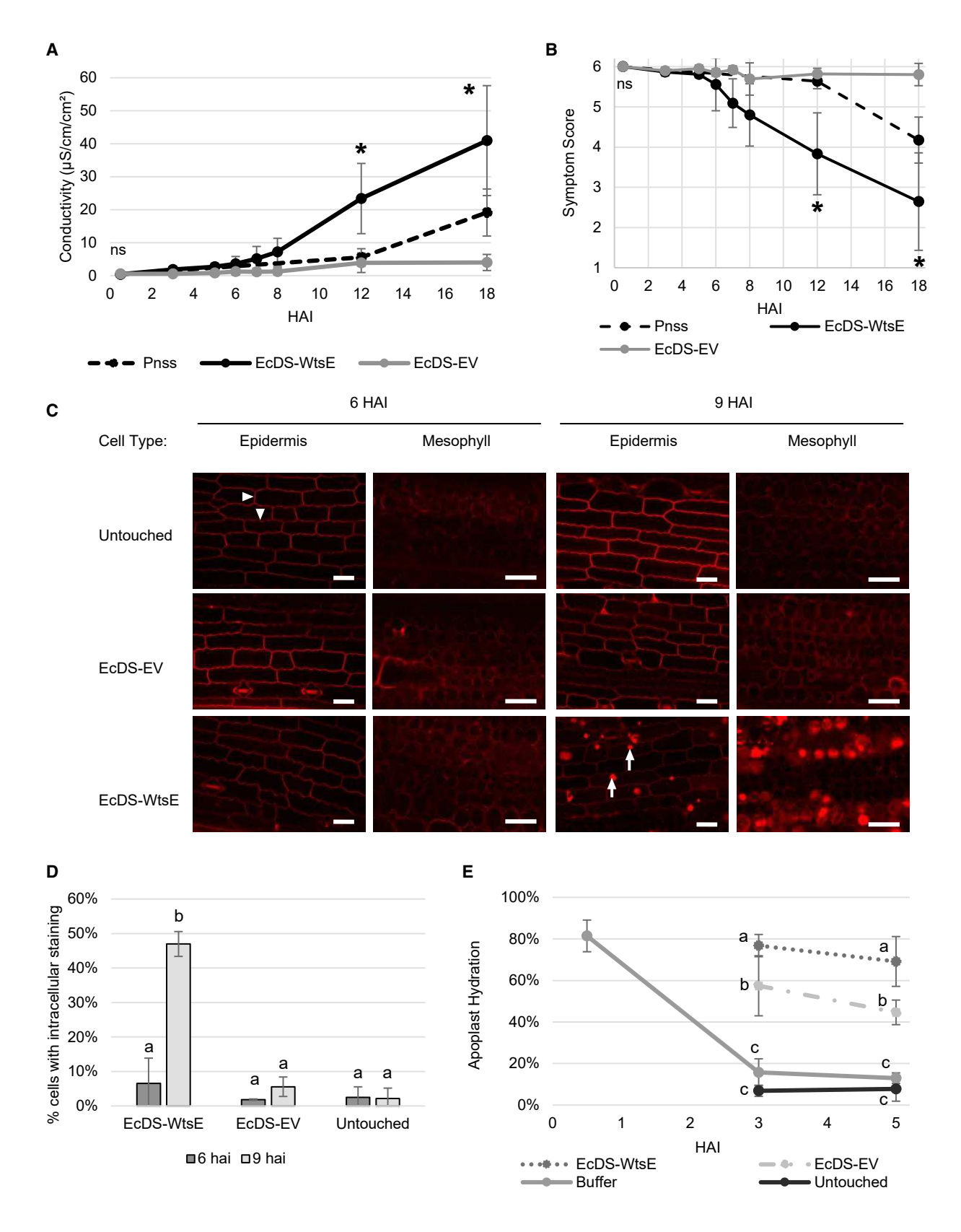
Using the EcDS, we sought to examine the effect of WtsE on the apoplast prior to its induction of necrosis. Thus, we first

pmols utilizable apoplast amino acids pmols utilizable apoplast N

 \times pmols bacterially assimilated N = estimated pmols consumed amino acids



Cell Host & MicrobeArticle



(legend on next page)

Article



established the timing of ion leakage (Figure 5A) and disease symptoms (Figure 5B). In both assays, EcDS-WtsE induced responses that were absent with EcDS-EV, and this appeared sooner than those induced by Pnss WT. The more rapid timing of responses with EcDS may result from constitutive expression of the type III secretion system and WtsE in EcDS versus their in planta induction in Pnss following infiltration. Based on the timing of these symptoms, PI staining was used to directly assess cellular integrity following infiltration with EcDS-EV or EcDS-WtsE (Figure 5C). At both 6 and 9 HAI, the appearance of epidermal and mesophyll cells of the leaves infiltrated with EcDS-EV did not differ from the untouched leaves. Following infiltration with EcDS-WtsE, both cell types also appeared normal at 6 HAI but displayed disintegrity by 9 HAI. Quantification of intracellular PI staining confirmed the observed patterns (Figure 5D). Based on these results, the ability of WtsE delivered by the EcDS to drive apoplast hydration without disrupting hostcell integrity was tested prior to 6 HAI (Figure 5E). Measurements of apoplast hydration revealed that water introduced into the apoplast during the infiltration of buffer or EcDS-EV was drying by 3 and 5 HAI. However, the apoplast of leaves infiltrated with EcDS-WtsE remained hydrated to a level significantly greater than that observed for EcDS-EV at both 3 and 5 HAI. Thus, WtsE is sufficient to promote apoplast hydration prior to disrupting the integrity of the maize cells and in the absence of other virulence factors of Pnss.

Next, we sought to determine the effect of WtsE, in the absence of other virulence factors of Pnss, on the abundance and partitioning of host metabolites. As discussed above, assimilation by proliferating Pnss partially obscures these effects of WtsE. Unlike Pnss, EcDS-WtsE and EcDS-EV do not proliferate in maize leaves; the number of each strain was constant at 0, 6, and 12 HAI (Figure 6A). Thus, relative to Pnss, using EcDS to deliver WtsE will minimize the confounding effects resulting from bacterial assimilation.

The whole leaf abundance of AAs, sugars, and OAs increased in maize leaves at 6 HAI with EcDS-WtsE, relative to EcDS-EV (Figure 6B). This finding, which mirrors the increase in the total levels of metabolites more than keeping pace with bacterial assimilation during Pnss infection, indicates that assimilation by Pnss likely obscured the effects of WtsE on overall metabolite abundances (Figures 3A and 3B). Indeed, WtsE induces the transcription of numerous genes involved with N and C metabolic processes (Asselin et al., 2015). WtsE delivered by EcDS also significantly increased the abundance of all four metabolite classes (AAs, sugars, OAs, and PCs) in the apoplast at 6 HAI (Figure 6C). The observed profile of AAs in the apoplast differed from that observed when cells were disrupted with DMSO, indicating that leakage from damaged maize cells does not account for the observed accumulation of metabolites in the apoplast following the delivery of WtsE by EcDS (Figure S4A). Also, increases in the overall metabolites levels do not solely account for their WtsE-induced increase in the apoplast. Rather, the partitioning of all four metabolite classes into the apoplast was significantly increased at 6 HAI with the EcDS-WtsE, relative to either EcDS-EV or buffer (Figure 6D). Notably, the percent of all four metabolite classes in the apoplast at 6 HAI with EcDS-WtsE was higher than that at 7 HAI with Pnss WT (compare Figure 7D and Figure 3E). Most strikingly and consistent with AAs being the metabolite class most dynamically assimilated by the proliferating Pnss, AAs were more than 60% apoplastic at 6 HAI with EcDS-WtsE versus less than 20% at 7 HAI with Pnss WT. Similarly, the WtsE-dependent partitioning of sugars and OAs into the apoplast following the delivery with EcDS is consistent with bacterial assimilation having obscured their dynamic accumulation in the apoplast when WtsE was delivered by Pnss.

We speculated that metabolites made available in the apoplast by WtsE are sufficient to account for the observed levels of N and C assimilations by Pnss. To test this prediction, the abundance of N or C in utilizable metabolites in the apoplast of the untouched leaves was subtracted from that in the leaves at 6 HAI with EcDS-WtsE. Remarkably, these values closely approximated the amount of N or C assimilated by Pnss WT by 12 HAI (Figure 6E), which was determined by subtracting the amount of N or C in the inoculum from that in Pnss WT isolated from infected plants (Figures 4D and 4E). Although a crude comparison between the two systems of WtsE delivery and at different time points that precede the WtsE-induced loss of maize cell integrity for each system, the results indicate that nutrient mobilization by WtsE occurs on a scale that can account for the level of assimilation by Pnss.

The level of individual metabolites accumulating in the apoplast following the delivery of WtsE by Pnss versus EcDS provides "fingerprints" that reveal the dynamic relationship between their arrival into the apoplast and, in the case of Pnss, their assimilation. We determined the percent that individual AAs,

Figure 5. Induction of apoplast hydration by WtsE independent of Pnss

(A) Ion leakage measurements of maize leaves following infiltration with Pnss WT, EcDS-WtsE, and EcDS-EV with standard deviation. Data are from three biological replicates, each treatment consisting of 2-8 technical replicates (n = 6-15). Asterisks indicate significant differences between EcDS-WtsE and Pnss WT as assessed by Student's t test at 0, 12, and 18 HAI where p < 0.05 and ns = not significant.

- (B) Symptom scores for EcDS-WtsE and EcDS-EV compared with Pnss WT, where a score of 1 indicates severe symptoms and a score of 6 indicates no symptoms. Error bars are standard deviation from the same three biological replicates in (A) with 4-16 leaves scored per replicate (n = 12-30). Asterisks indicate significant differences between EcDS-WtsE and Pnss WT as assessed by Student's t test at 0, 12, and 18 HAI where p < 0.05 and ns = not significant.
- (C) Confocal microscopy images of propidium iodide (PI) maize epidermal and mesophyll cells at 6 and 9 HAI with EcDS-WtsE, EcDS-EV, or untouched plants. Arrowheads and arrows indicate the staining of cell walls and intracellular structures, respectively. Scale bars, 100 µm.
- (D) Quantification of intracellular PI staining in epidermal cells of data represented in (C). Data are from two biological replicates and error bars are standard deviations between replicates. The number of cells counted for EcDS-WtsE, EcDS-EV, and untouched were 1,664, 1,101, and 978 at 6 HAI and 1,501, 1,070, and 1,215 at 9 HAI, respectively. Different letters indicate statistical significance via ANOVA and Tukey's HSD test across all treatments and time points where p < 0.05.
- (E) Apoplast hydration of maize leaves following the infiltration with EcDS-WtsE, EcDS-EV, or buffer and in untouched plants with standard error. Six to eight leaves were assessed individually at each time point within each of three biological replicates. Different letters indicate significance between treatments at each time point via ANOVA and Tukey's HSD test where p < 0.05.



Cell Host & MicrobeArticle

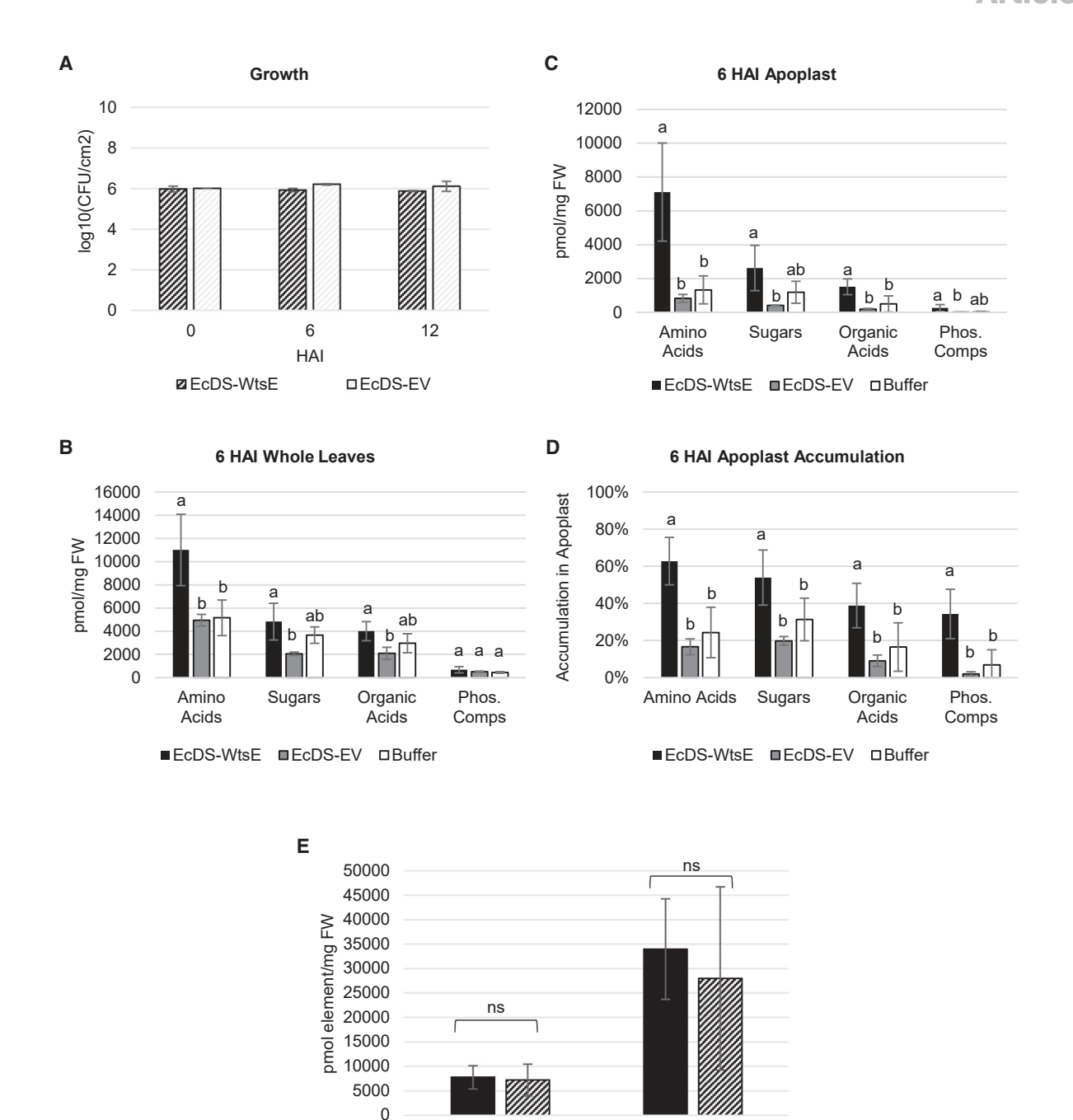


Figure 6. Effect of WtsE on abundance and partitioning into the apoplast of metabolite classes

(A) Growth of EcDS-WtsE and EcDS-EV following the infiltration into maize leaves with standard deviation.

(B–D) Maize plants were infiltrated with EcDS-WtsE, EcDS-EV, or buffer, and metabolite composition of the apoplast fluids and remaining leaves after apoplast removal were assessed at 6 HAI. (B) and (C) show abundance of the indicated metabolite classes in the whole leaves and apoplast, respectively. (D) shows the percentage of each metabolite class from the whole leaves that are present in the apoplast. Error bars are standard deviation from four biological replicates, each comprising one technical replicate (n = 4). Letters represent significance assessed by ANOVA followed by Tukey's HSD test where p < 0.05.

■ Pnss assimilation in 12 HAI Increase by EcDS-WtsE in 6 HAI

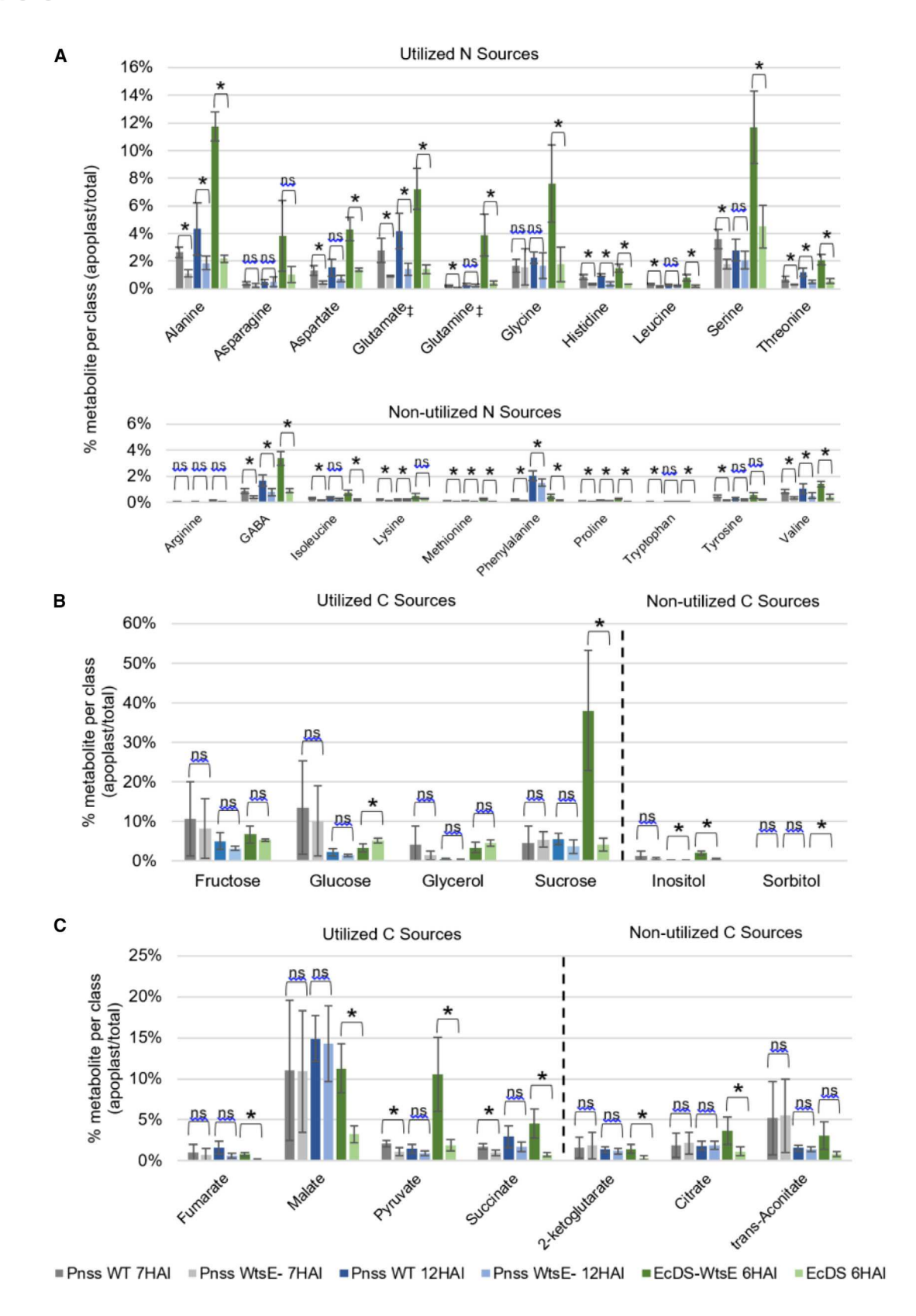
Carbon

Nitrogen

(E) Quantities of N or C assimilated by the proliferating Pnss at 12 HAI (difference between bacteria isolated at 12 HAI and inoculated bacteria) compared with the apoplast accumulation of utilizable N or C at 6 HAI with EcDS-WtsE (levels measured following EcDS-WtsE infiltration minus those at 7 HAI in untouched leaves). Error bars are standard deviation from three (*Pnss* elemental analysis) or four (EcDS-WtsE metabolomics) replicates and differences were assessed by Student's t test where p < 0.05 and ns = not significant.







(legend on next page)



sugars, and OAs in the apoplast comprised of their total metabolite class in the whole leaf (Figure 7). The differences between Pnss ± WtsE indicate that WtsE-dependent accumulation in the apoplast was offset by comparable levels of consumption by Pnss WT and Pnss WtsE- at 7 HAI and by a higher level of consumption by Pnss WT, relative to Pnss WtsE-, at 12 HAI (see Figures 1C and 4). The difference between EcDS ± WtsE at 6 HAI indicates WtsE-dependent accumulation in the apoplast in the absence of significant consumption by EcDS (see Figure 6A). These fingerprints differ markedly between individual AAs (Figure 7A). Asn, Gln, Gly, and Ser display WtsE-dependent increases with EcDS that are absent or minimal with Pnss at either time point. Ala, Asp, and Glu also display exaggerated accumulation in the apoplast when WtsE is delivered by EcDS, relative to Pnss. Notably, these 7 AAs, which account for 80% of the AAs localized in the apoplast following the infiltration with EcDS-WtsE, are among the 9 AAs most efficiently utilized by Pnss as a sole source of N (Figure 4A). The convergence of these findings further supports the prediction that Pnss growth in the apoplast is limited by the availability of these preferred sources of N. Strikingly, the fingerprints for sugars reveal that, when delivered by non-proliferating EcDS, WtsE induces a dramatic increase in apoplast accumulation of sucrose (Figure 7B). The modest accumulation of sugars other than sucrose in the apoplast of the leaves infiltrated with Pnss decreases at 12 HAI, relative to 7 HAI, likely reflecting opportunistic consumption following availability due to the "buffer effect" and/or the activity of the single-cell wall degrading enzyme encoded by Pnss (Mohammadi et al., 2012). Lastly, the fingerprints for OAs reveal WtsE-induced accumulation of malate, pyruvate, and succinate (Figure 7C), which are each efficiently utilized as a sole source of C by Pnss (Figure 4A). These findings indicate that the assumption underlying Figure 4F that Pnss consumes utilizable metabolites proportionally to their availability in the apoplast at 12 HAI is likely flawed. Rather, select metabolites, such as Ala, Gln, Ser, sucrose, and pyruvate, likely move from inside maize cells to the apoplast to Pnss-assimilate at more rapid rates. Nonetheless, the trends presented in Figure 4F remain valid. And the observation that, in the absence of assimilation, WtsE induces greater apoplast accumulation of metabolites that are preferred nutrients of Pnss further supports our conclusion that a dynamic balance between nutrient availability and consumption occurs during biotrophic proliferation of *Pnss* in its maize host.

DISCUSSION

Water availability is critical for the growth of bacterial pathogens inside their plant hosts. At an environmental scale, disease outbreaks are associated with high humidity, and at the tissue level, local desiccation at sites of infection is a facet of plant immune defense (Beattie, 2011). The need of pathogens to suppress host immunity is well established, and a plethora of T3Es have

been shown to inhibit host defense (Asai and Shirasu, 2015; Jones and Dangl, 2006). However, the growth of *P. syringae* lacking WS-inducing effectors, including an AvrE-family T3E, in immunocompromised Arabidopsis plants remained dependent on apoplast hydration (Xin et al., 2016). By demonstrating here that high-level growth of *Pnss* in susceptible maize plants is preceded by WtsE-induced apoplast hydration, this work further supports the importance of water availability for the proliferation of phytopathogenic bacteria. Additionally, through establishing the timing of WtsE-induced responses, we demonstrate that apoplast hydration and *Pnss* proliferation precede the disruption of host-cell integrity and necrosis. Thus, WS does not result from the leakage of cytosolic contents at the onset of necrosis but rather is actively induced during the biotrophic phase of infection.

In addition to water availability, the acquisition of nutrients is critical for the growth of plant pathogens. During biotrophy, some fungal and oomycete pathogens obtain nutrients through the formation of haustoria, feeding structures that provide intimate contact via invaginations into living plant cells. Necrotrophic pathogens, on the other hand, obtain nutrients from dying and dead plant cells. For hemibiotrophic bacteria, it is unclear whether the nutrients available in the apoplast of an uninfected plant are sufficient to support the high level of proliferation observed during the biotrophic phase of infection, which happens prior to necrosis. For example, P. syringae pv. tomato feeds on nutrients that are abundant in the apoplast of uninfected tomato plants (Rico and Preston, 2008). The discovery that TAL effectors contribute to the virulence of Xanthomonas spp. by inducing the expression of nutrient transporters indicates the importance of liberating nutrients from within host cells. However, whether the TAL effectors promote susceptibility by overcoming defense-induced nutrient uptake or increasing nutrient availability above pre-infection levels is unknown. Our findings indicate that high-level growth of Pnss in the maize apoplast depends on the dynamic mobilization of nutrients, in the form of AAs, sugars, and OAs, from intact maize cells to the apoplast where they are assimilated by proliferating bacteria. Specifically, our estimates indicate that, relative to uninfected leaves, the apoplast of the leaves at 12 HAI with Pnss contains >40- and >13-fold more utilizable/assimilated N and C of which >70% and >40% has already been assimilated by the pathogen. Consistent with the dynamic relationship between nutrient availability and assimilation, genes encoding transporters and metabolic enzymes were found to be critical for the fitness of Pnss in the xylem of infected maize plants (Duong et al., 2018). The broad distribution of AvrE-family effectors indicates that promoting water and nutrient availability during the biotrophic phase of infection is important for plant pathogenic bacteria from multiple genera. Furthermore, similarities between the phenotypic outputs of AvrE-family effectors and TAL effectors point to an essential role of actively induced nutritional susceptibility in phytopathogenic bacteria.

Figure 7. Fingerprinting of metabolite arrival into and consumption from the apoplast

Percentage of individual metabolites in the apoplast, relative to the whole leaf quantity of their metabolite class, following the infiltration with *Pnss* WT and *Pnss* WtsE— at 7 and 12 HAI and with EcDS-WtsE and EcDS-EV at 6 HAI.

(A–C) AAs sources of N (A) and sugar and OA sources of C (B and C, respectively) are separated into utilizable and non-utilizable groups as determined in Figure 4A. Barbells (‡) denote AAs that are efficiently utilized as C sources by *Pnss* WT. Error bars are standard deviation from four biological replicates, each comprising one technical replicate (n = 4). Asterisks indicate significant differences as assessed by Student's t test where p < 0.05 and ns = not significant.

Article



Nutrient acquisition and WS appear to be intertwined phenomena. The buffer effect, perhaps analogous to the initial stages of apoplast hydration, leads to increased abundance of water-soluble metabolites in the apoplast. Mobilization of nutrients into hydrated apoplastic space may account for the outgrowth of non-pathogenic, endophytic bacteria in the water-soaked leaves of immunocompromised Arabidopsis plants (Xin et al., 2016). However, it is apparent that WtsE drives more metabolites to the apoplast than can be accounted for by the buffer effect. In addition to serving as nutrients for Pnss, the accumulating metabolites may promote apoplast hydration by increasing water potential in the apoplast, as noted for the TAL effector AvrHah1 (Schwartz et al., 2017). In such a scenario, the extent of apoplast hydration would be governed by the dynamic balance between the accumulation of metabolites, acting as solutes, in the apoplast and their assimilation, as nutrients, by the proliferating bacteria. Indeed, WtsE delivered by non-proliferating EcDS causes an exaggerated accumulation of metabolites in the apoplast, as well as earlier apoplast hydration and macroscopic WS. Therefore, we propose that, by promoting the movement of metabolites and possibly also water across the intact membranes of maize cells, WtsE tips the balance in favor of a feedforward relationship promoting the accumulation of both water and metabolites in the apoplast. Furthermore, the early timing of these physiological perturbations raises the possibility that the accumulation of water and/or metabolites in the apoplast underlies other functional outputs of AvrE-family and TAL effectors, including the suppression of host defense and induction of necrosis. The more rapid necrosis observed when WtsE is delivered by EcDS, compared with when it is delivered by Pnss, is consistent with runaway modification of the apoplast leading to necrosis.

The mechanism by which WtsE causes metabolites to move from intact plant cells to the apoplast is unknown. Possibly underlying the broad spectrum of AAs whose partitioning is affected by WtsE is the expansive repertoire of AA transporters encoded in plant genomes and their broad substrate specificity (Kim et al., 2021). The more specific effect of WtsE on the partitioning of sucrose points to a potential role of clade 3 members of the SWEET family of sugar transporters (Kim et al., 2021). WtsE may indirectly target these transporters via its direct interaction with the isoforms of protein phosphatase 2A and receptor-like kinases (RLKs) at the maize plasma membrane (Jin et al., 2016). Similarly, WtsE may indirectly target aquaporins to influence water movement. Indeed, RLKs directly targeted by WtsE in maize and DspA/E, the AvrE-family T3E of the fire blight pathogen Erwinia amylovora, in apple are homologs of Arabidopsis RKL1, which regulates aquaporin activity (Bellati et al., 2016; Jin et al., 2016; Meng et al., 2006). Notably, AvrE1 from P. syringae has recently been shown to co-localize with Arabidopsis aquaporins in plasma membrane microdomains (Xin et al., 2021). Regardless of the mechanism, this work establishes dynamic modification of the plant apoplast as critical to the nutritional susceptibility of maize to Pnss, a finding that is likely generalizable across phytopathogenic bacteria.

STAR*METHODS

Detailed methods are provided in the online version of this paper and include the following:

- KEY RESOURCES TABLE
- RESOURCE AVAILABILITY
 - Lead contact
 - Materials availability
 - Data and code availability
- EXPERIMENTAL MODEL AND SUBJECT DETAILS
 - Maize
 - O Pantoea stewartii subsp. stewartii
 - O E. coli
- METHOD DETAILS
 - Vacuum infiltration
 - In planta bacterial growth assay
 - Ion leakage
 - Malate dehydrogenase activity
 - Apoplast extraction
 - Detached leaf assay
 - Liquid Chromatography Tandem Mass Spectrometry (LC-MS/MS)
 - Confocal microscopy
 - Maize kernel protein quantification
 - Elemental analysis
- QUANTIFICATION AND STATISTICAL ANALYSIS

SUPPLEMENTAL INFORMATION

Supplemental information can be found online at https://doi.org/10.1016/j. chom.2022.03.017.

ACKNOWLEDGMENTS

The authors thank Anya Dobritsa for access and support of confocal microscopy, the BioAnalytical Facility at the University of North Texas for access to the LC-MS/MS equipment, and Jonathan Jacobs for the use of the plate reader. Support for I.G. came from the Translational Plant Sciences Graduate Program and from a National Institute of Food and Agriculture AFRI-ELI predoctoral fellowship (award no. 2017-67011-26080). The work was also supported by grants to D.M. from the US Department of Agriculture (National Institute of Food and Agriculture, grant no. 2015-11870612), the National Science Foundation (Division of Integrative Organismal Systems, grant no. 1953509), and the Next-Generation BioGreen 21 program of the Korean RDA (SSAC, grant no. PJ01326904).

AUTHOR CONTRIBUTIONS

I.G., A.P.A., and D.M. conceptualized the project. A.P.A. and D.M. supervised the research. I.G., L.G., G.E., K.M., W.Z., and J.-C.C. performed experiments. All authors contributed to data analysis. I.G. and D.M. developed the figures and wrote the original draft, with review and editing contributions from L.G., G.E., K.M., J.-C.C., and A.P.A. to the final paper. I.G. and D.M. acquired funding to support the project.

DECLARATION OF INTERESTS

The authors declare no competing interests.

Received: October 8, 2021 Revised: February 9, 2022 Accepted: March 10, 2022 Published: April 13, 2022

REFERENCES

Asai, S., and Shirasu, K. (2015). Plant cells under siege: plant immune system versus pathogen effectors. Curr. Opin. Plant Biol. 28, 1-8.



Asselin, J.E., Lin, J., Perez-Quintero, A.L., Gentzel, I., Majerczak, D., Opiyo, S.O., Zhao, W., Paek, S.-M.M., Kim, M.G., Coplin, D.L., et al. (2015). Perturbation of maize phenylpropanoid metabolism by an AvrE family type III effector from Pantoea stewartii. Plant Physiol. 167, 1117-1135.

Aung, K., Jiang, Y., and He, S.Y. (2018). The role of water in plant-microbe interactions. Plant J. 93, 771-780.

Beattie, G.A. (2011). Water relations in the interaction of foliar bacterial pathogens with plants. Annu. Rev. Phytopathol. 49, 533-555.

Bellati, J., Champeyroux, C., Hem, S., Rofidal, V., Krouk, G., Maurel, C., and Santoni, V. (2016). Novel aquaporin regulatory mechanisms revealed by interactomics. Mol. Cell. Proteomics 15, 3473-3487.

Chen, L.Q., Hou, B.H., Lalonde, S., Takanaga, H., Hartung, M.L., Qu, X.Q., Guo, W.J., Kim, J.G., Underwood, W., Chaudhuri, B., et al. (2010). Sugar transporters for intercellular exchange and nutrition of pathogens. Nature 468,

Chong, J., Soufan, O., Li, C., Caraus, I., Li, S., Bourque, G., Wishart, D.S., and Xia, J. (2018). MetaboAnalyst 4.0: towards more transparent and integrative metabolomics analysis. Nucleic Acids Res. 46, W486-W494.

Cocuron, J.C., and Alonso, A.P. (2014). Liquid chromatography tandem mass spectrometry for measuring 13C-labeling in intermediates of the glycolysis and pentose-phosphate pathway. Methods Mol. Biol. 1090, 131-142.

Cocuron, J.C., Anderson, B., Boyd, A., and Alonso, A.P. (2014). Targeted metabolomics of Physaria fendleri, an industrial crop producing hydroxy fatty acids. Plant Cell Physiol. 55, 620-633.

Cocuron, J.C., Casas, M.I., Yang, F., Grotewold, E., and Alonso, A.P. (2019). Beyond the wall: high-throughput quantification of plant soluble and cell-wall bound phenolics by liquid chromatography tandem mass spectrometry. J. Chromatogr. A 1589, 93-104.

Coplin, D.L., Frederick, R.D., Majerczak, D.R., and Haas, E.S. (1986). Molecular cloning of virulence genes from Erwinia stewartii. J. Bacteriol. 168, 619-623.

De Souza, A.P., Cocuron, J.C., Garcia, A.C., Alonso, A.P., and Buckeridge, M.S. (2015). Changes in whole-plant metabolism during the grain-filling stage in sorghum grown under elevated CO2 and drought. Plant Physiol. 169, 1755-1765.

Degrave, A., Siamer, S., Boureau, T., and Barny, M.A. (2015). The AvrE superfamily: ancestral type III effectors involved in suppression of pathogen-associated molecular pattern-triggered immunity. Mol. Plant Pathol. 16, 899-905.

Dolph, P.J., Majerczak, D.R., and Coplin, D.L. (1988). Characterization of a gene cluster for exopolysaccharide biosynthesis and virulence in Erwinia stewartii. J. Bacteriol. 170, 865-871.

Duong, D.A., Stevens, A.M., and Jensen, R.V. (2018). Expanded analysis of the Pantoea stewartii subsp. stewartii DC283 complete genome reveals plasmidborne virulence factors. Preprint at bioRxiv. https://doi.org/10.1101/407825.

El Kasmi, F., Horvath, D., and Lahaye, T. (2018). Microbial effectors and the role of water and sugar in the infection battle ground. Curr. Opin. Plant Biol. 44, 98-107.

Frederick, R.D., Ahmad, M., Majerczak, D.R., Arroyo-Rodríguez, A.S., Manulis, S., and Coplin, D.L. (2001). Genetic organization of the Pantoea stewartii subsp. stewartii hrp Gene cluster and sequence analysis of the hrpA, hrpC, hrpN, and wtsE operons. Mol. Plant Microbe Interact. 14, 1213-1222.

Freeman, B.C., and Beattie, G.A. (2009). Bacterial growth restriction during host resistance to Pseudomonas syringae is associated with leaf water loss and localized cessation of vascular activity in Arabidopsis thaliana. Mol. Plant Microbe Interact. 22, 857-867.

Gaudriault, S., Malandrin, L., Paulin, J.P., and Barny, M.A. (1997). DspA, an essential pathogenicity factor of Erwinia amylovora showing homology with AvrE of Pseudomonas syringae, is secreted via the Hrp secretion pathway in a DspB-dependent way. Mol. Microbiol. 26, 1057-1069.

Gentzel, I., Giese, L., Zhao, W., Alonso, A.P., and Mackey, D. (2019). A simple method for measuring apoplast hydration and collecting apoplast contents. Plant Physiol. 179, 1265-1272.

Ham, J.H., Bauer, D.W., Fouts, D.E., and Collmer, A. (1998). A cloned Erwinia chrysanthemi Hrp (type III protein secretion) system functions in Escherichia coli to deliver Pseudomonas syringae Avr signals to plant cells and to secrete Avr proteins in culture. Proc. Natl. Acad. Sci. USA 95, 10206-10211.

Ham, J.H., Majerczak, D., Ewert, S., Sreerekha, M.V., Mackey, D., and Coplin, D. (2008). WtsE, an AvrE-family type III effector protein of Pantoea stewartii subsp. stewartii, causes cell death in non-host plants. Mol. Plant Pathol. 9, 633-643

Ham, J.H., Majerczak, D.R., Arroyo-Rodriguez, A.S., Mackey, D.M., and Coplin, D.L. (2006). WtsE, an AvrE-family effector protein from Pantoea stewartii subsp. stewartii, causes disease-associated cell death in corn and requires a chaperone protein for stability. Mol. Plant Microbe Interact. 19, 1092-1102.

Ham, J.H., Majerczak, D.R., Nomura, K., Mecey, C., Uribe, F., He, S.Y., Mackey, D., and Coplin, D.L. (2009). Multiple activities of the plant pathogen type III effector proteins WtsE and AvrE require WxxxE motifs. Mol. Plant Microbe Interact. 22, 703-712.

Jin, L., Ham, J.H., Hage, R., Zhao, W., Soto-Hernández, J., Lee, S.Y., Paek, S.M., Kim, M.G., Boone, C., Coplin, D.L., and Mackey, D. (2016). Direct and indirect targeting of PP2A by conserved bacterial Type-III effector proteins. PLoS Pathog. 12, e1005609.

Jones, J.D.G., and Dangl, J.L. (2006). The plant immune system. Nature 444,

Jones, K., Kim, D.W., Park, J.S., and Khang, C.H. (2016). Live-cell fluorescence imaging to investigate the dynamics of plant cell death during infection by the rice blast fungus Magnaporthe oryzae. BMC Plant Biol. 16, 69.

Kim, H.S., Thammarat, P., Lommel, S.A., Hogan, C.S., and Charkowski, A.O. (2011). Pectobacterium carotovorum elicits plant cell death with DspE/F but the P. carotovorum DspE does not suppress callose or induce expression of plant genes early in plant-microbe interactions. Mol. Plant Microbe Interact.

Kim, J.Y., Loo, E.P.-I., Pang, T.Y., Lercher, M., Frommer, W.B., and Wudick, M.M. (2021). Cellular export of sugars and amino acids: role in feeding other cells and organisms. Plant Physiol. 187, 1893-1914.

Kvitko, B.H., Park, D.H., Velásquez, A.C., Wei, C.F., Russell, A.B., Martin, G.B., Schneider, D.J., and Collmer, A. (2009). Deletions in the repertoire of Pseudomonas syringae pv. tomato DC3000 type III secretion effector genes reveal functional overlap among effectors. PLoS Pathog. 5, e1000388.

Langlotz, C., Schollmeyer, M., Coplin, D.L., Nimtz, M., and Geider, K. (2011). Biosynthesis of the repeating units of the exopolysaccharides amylovoran from Erwinia amylovora and stewartan from Pantoea stewartii. Physiol. Mol. Plant Pathol. 75, 163-169.

Meng, X., Bonasera, J.M., Kim, J.F., Nissinen, R.M., and Beer, S.V. (2006). Apple proteins that interact with DspA/E, a pathogenicity effector of Erwinia amylovora, the fire blight pathogen. Mol. Plant Microbe Interact. 19, 53-61.

Mitchell, K., Brown, I., Knox, P., and Mansfield, J. (2015). The role of cell wallbased defences in the early restriction of non-pathogenic hrp mutant bacteria in Arabidopsis. Phytochemistry 112, 139-150.

Mohammadi, M., Burbank, L., and Roper, M.C. (2012). Pantoea stewartii subsp. stewartii produces an endoglucanase that is required for full virulence in sweet corn. Mol. Plant Microbe Interact. 25, 463-470.

Mor, H., Manulis, S., Zuck, M., Nizan, R., Coplin, D.L., and Barash, I. (2001). Genetic organization of the hrp gene cluster and dspAE/BF operon in Erwinia herbicola pv. gypsophilae. Mol. Plant Microbe Interact. 14, 431-436.

Mouginot, C., Kawamura, R., Matulich, K.L., Berlemont, R., Allison, S.D., Amend, A.S., and Martiny, A.C. (2014). Elemental stoichiometry of fungi and bacteria strains from grassland leaf litter. Soil Biol. Biochem. 76, 278-285.

Naseem, M., Kunz, M., and Dandekar, T. (2017). Plant-pathogen maneuvering over apoplastic sugars. Trends Plant Sci. 22, 740-743.

Pataky, J.K. (2003). Stewart's Wilt of Corn (American Phytopathological

Rico, A., and Preston, G.M. (2008). Pseudomonas syringae pv. tomato DC3000 uses constitutive and apoplast-induced nutrient assimilation pathways to catabolize nutrients that are abundant in the tomato apoplast. Mol. Plant Microbe Interact. 21, 269-282.

Article



Roper, M.C. (2011). Pantoea stewartii subsp. stewartii: lessons learned from a xylem-dwelling pathogen of sweet corn. Mol. Plant Pathol. 12, 628-637.

Roper, M.C., Burbank, L.P., Williams, K., Viravathana, P., Tien, H.Y., and Von Bodman, S. (2015). A large repetitive RTX-like protein mediates water-soaked lesion development, leakage of plant cell content and host colonization in the Pantoea stewartii subsp. stewartii Pathosystem. Mol. Plant Microbe Interact. 28. 1374-1382.

Schwartz, A.R., Morbitzer, R., Lahaye, T., and Staskawicz, B.J. (2017). TALEinduced bHLH transcription factors that activate a pectate lyase contribute to water soaking in bacterial spot of tomato. Proc. Natl. Acad. Sci. USA 114,

Sonawala, U., Dinkeloo, K., Danna, C.H., McDowell, J.M., and Pilot, G. (2018). Review: functional linkages between amino acid transporters and plant responses to pathogens. Plant Sci. 277, 79-88.

Wagner, S., Grin, I., Malmsheimer, S., Singh, N., Torres-Vargas, C.E., and Westerhausen, S. (2018). Bacterial type III secretion systems: a complex device for the delivery of bacterial effector proteins into eukaryotic host cells. FEMS Microbiol. Lett. 365, fny201.

Wright, C.A., and Beattie, G.A. (2004). Pseudomonas syringae pv. tomato cells encounter inhibitory levels of water stress during the hypersensitive response of Arabidopsis thaliana. Proc. Natl. Acad. Sci. USA 101, 3269-3274.

Xin, X.-F., Kinch, L., Cai, B., Paasch, B.C., Kvitko, B., Grishin, N.V., and He, S.Y. (2021). Pseudomonas syringae effector AvrE associates with plant membrane nanodomains and binds phosphatidylinositides in vitro. Preprint at bioRxiv. 2021.07.08.451616.

Xin, X.F., Nomura, K., Aung, K., Velásquez, A.C., Yao, J., Boutrot, F., Chang, J.H., Zipfel, C., and He, S.Y. (2016). Bacteria establish an aqueous living space in plants crucial for virulence. Nature 539, 524-529.

Yamada, K., Saijo, Y., Nakagami, H., and Takano, Y. (2016). Regulation of sugar transporter activity for antibacterial defense in Arabidopsis. Science 354, 1427-1430.



STAR*METHODS

KEY RESOURCES TABLE

REAGENT or RESOURCE	SOURCE	IDENTIFIER
Bacterial and Virus Strains		
Pantoea stewartii subsp. stewartii, wild-type DC283	Coplin et al., 1986	NCBI:txid660596
Pantoea stewartii subsp. stewartii, WtsE null mutant DM5101	Ham et al., 2006	N/A
Pantoea stewartii subsp. stewartii, WxxxE mutant JH039	Ham et al., 2009	N/A
E. coli MC4100: EcDS (pCPP2156 + pLAFR3)	Asselin et al., 2015	N/A
E. <i>coli</i> MC4100: EcDS-WtsE (pCPP2156 + pJA001)	Asselin et al., 2015	N/A
Critical Commercial Assays		
Malate Dehydrogenase Assay Kit	Millipore Sigma	MAK196-1KT
DC Protein Assay Kit	Bio-Rad	5000112
Experimental Models: Organisms/Strains		
Zea mays: B73	Mackey lab stock	https://www.maizegdb.org/ data_center/stock?id=47638

RESOURCE AVAILABILITY

Lead contact

Requests for further information, resources and reagents should be directed to the lead contact, David Mackey (mackey.86@ osu.edu).

Materials availability

This study did not generate new unique reagents.

Data and code availability

- All data reported in this paper will be shared by the lead contact upon request.
- This paper does not report original code.
- Any additional information required to reanalyze the data reported in this paper is available from the lead contact upon request.

EXPERIMENTAL MODEL AND SUBJECT DETAILS

Maize

B73 maize ($Zea\,mays$) or Seneca Horizon sweet corn seedlings were grown in a Conviron growth chamber set to 30°C with an 18-hour light (\sim 95 μ E m⁻² s⁻¹) / 6-hour dark cycle. Ten to twelve seeds were planted per round 4-inch pot with Sungro MetroMix soil and watered every 36-48 hours or as needed. One to four hours prior to vacuum infiltration, plants were watered and humidity elevated to at least 65% with a humidifier. Six-day-old plants that did not have fully expanded first true leaves were discarded prior to vacuum infiltration. Vacuum infiltrations were performed approximately 5-6 hours into the light period.

Pantoea stewartii subsp. stewartii

Pantoea stewartii subsp. stewartii (Pnss) strains were grown on lysogeny broth (LB) solid media supplemented with 20 μg/mL nalidixic acid (DC283 (Coplin et al., 1986), wild-type strain, referred to as Pnss WT; JH039 (Ham et al., 2009), DC283-derived WtsE-W694A/W840A mutant strain, referred to as Pnss Δw12) or 20 μg/mL kanamycin (DM5101; Ham et al., 2006, DC283-derived mutant strain with non-polar deletion of WtsE, referred to as Pnss WtsE-) at 28°C. For vacuum infiltration experiments, Pnss was grown in LB liquid media overnight, subcultured at a 1:10 dilution, and grown for approximately four additional hours until reaching an optical density of 0.7 at 540 nm.

For assays of *Pnss* growth using sole sources of C or N, *Pnss* WT was grown overnight in LB liquid medium supplemented with 20 µg/mL nalidixic acid. Cells were then subcultured at a 1:5 dilution in IM5.5 minimal medium (Frederick et al., 2001) for approximately six hours prior to harvest by centrifugation at 5000 x g for 5 minutes at room temperature and washing with sterile water to remove residual liquid medium. To analyze specific C sources, casamino acids and sucrose were removed from IM5.5 media.

Article



To analyze specific N sources, casamino acids and ammonium sulfate were removed from IM5.5 media. Cells were resuspended in these modified IM5.5 media to an OD of 0.2 at 550 nm. This suspension was then diluted a further tenfold into modified IM5.5 minimal media containing the C or N source of interest. Each culture was distributed into 6 wells of 100 μ L each on a 96-well flat-bottom plate, which was then sealed with a Breathe-Easy membrane (Diversified Biotech #BEM-1). A Wallac Victor² 1420 Multilabel Counter was used to measure absorbance at 550 nm every thirty minutes over ten hours, with orbital shaking at max speed at 28°C between readings. Absorbance readings were corrected back to optical density at 550 nm by a standard curve. pH readings of individual media were obtained with a handheld Horiba Laquatwin pH meter.

E. coli

E. coli delivery system strains (EcDS) (MC4100 strain with cosmid pCPP2156 containing *Dickeya dadantii* TTSS; Ham et al., 1998), which contained a second plasmid carrying WtsE and its WtsF chaperone (pJA001, referred to as EcDS-WtsE) or the empty vector (pLAFR3, referred to as EcDS-EV) were grown at 28°C in LB supplemented with both 5 μg/mL tetracycline and 50 μg/mL spectinomycin (pJA001 and pLAFR3 plasmids described in Asselin et al., 2015). For vacuum infiltrations, EcDS strains were grown overnight in liquid LB and then sub-cultured at a 1:10 dilution until reaching an optical density of 1.0 at 600 nm.

METHOD DETAILS

Vacuum infiltration

As described in Asselin et al. (2015), *Pnss* subcultures at a 540 nm optical density of 0.7 or EcDS cells at a 600 nm optical density of 1.0 were harvested by centrifugation at 3795 x g for 12 min at room temperature. To make a high-titer inoculum (3.5x10⁸ CFU/mL), *Pnss* cell pellets were resuspended in 10 mM potassium phosphate buffer (pH 7.2) with 0.2% Tween-40 to a 540 nm optical density of 0.57. EcDS cells were resuspended in 10 mM potassium phosphate buffer (pH 7.2) with 0.2% Tween-40 to a 600 nm optical density of 1.0. For vacuum infiltrations, plants were inverted into beakers containing 300 mL 10 mM potassium phosphate buffer with 0.2% Tween-40 (control) or bacterial inoculum. Using a Nalgene vacuum chamber, up to three pots at a time were subjected to a vacuum of 500 mmHg for 5 min, followed by vacuum release. This was repeated two more times for a total of 15 min. Plants were then allowed to air dry for 10–15 min until their return to the growth chamber with relative humidity at 65%–70%.

In planta bacterial growth assay

Six-day-old maize seedlings were vacuum infiltrated with high-titer *Pnss*. Plants were returned to the growth chamber after inoculum had air-dried for 10–15 min at room temperature. At each collection time-point, three first-true-leaf tips were excised (~4–5-cm lengths) and two 1-cm diameter disks per leaf were collected with a cork borer. Both leaf disks were then placed in a 1.5 mL microfuge tube containing 1 mL cold sterile ddH₂O and two 3.2-mm stainless steel beads. Samples were kept on ice until all collections had been made for that time-point. Next, the leaf disks were homogenized with a TissueLyser (Qiagen) bead beater for 60 seconds at 30 Hz. Upon visual verification of complete homogenization (with an additional 30 seconds in the bead beater, if necessary), triplicate portions of the leaf-water suspension were serially diluted in sterile water and plated with a replicator tool onto solid LB media containing appropriate antibiotics. Plates were allowed to dry for 20 min before being inverted and incubated at 28°C for two days. Resulting colony number counts were converted to CFU/leaf area (cm²) and transformed to a log₁₀ scale.

Ion leakage

Six-day-old maize seedlings were vacuum infiltrated with high-titer Pnss, or the buffer-only control (10 mM KPO₄ with 0.2% Tween-40). Plants were returned to the growth chamber after inoculum had air-dried for 10–15 min at room temperature. At each collection time-point, two leaf tips were excised, their margins traced onto paper for leaf area calculation, and submerged in 30 mL ddH₂O for 45 min at room temperature with occasional gentle agitation. Two replicates were completed for each treatment at each time-point. Untouched leaves were sampled to determine background conductivity, including that due to leaf excision. After incubation, leaves were removed and conductivity of the solution measured with a WTW Cond 330i meter and TetraCon 325 probe. Conductivity values (μ S/cm) were background-corrected by subtraction of the blank (ddH₂O) value and divided by leaf area (cm²).

Malate dehydrogenase activity

Six-day-old maize seedlings were vacuum infiltrated with buffer, 5% DMSO or high-titer *Pnss* WtsE- or *Pnss* WT. After apoplast isolation, apoplast samples were spun again at 5000 rcf for 10 min at 4°C and supernatant was transferred to a new tube and snap frozen in liquid nitrogen. After weighing residual leaves, a 0.8 cm² leaf punch was collected from each leaf and these punches were weighed and snap frozen in liquid nitrogen. MDH activity was measured using the Malate Dehydrogenase Assay Kit (MAK196) from Sigma Aldrich in a 96 well plate according to manufacturer's instructions. Sample dilutions were done in MDH assay buffer, with the apoplast fluid at 1:10 and the leaf tissue at 1:1000. The plate was incubated at 37°C and read at 450 nm every 10 min for 120 min. MDH activity was consistent across the time course and was calculated from the 30-minute readings according to manufacturer's instructions.

Apoplast extraction

Apoplast fluid was collected as described in Gentzel et al. (2019). Briefly, maize seedling first-true-leaf tips were weighed to acquire the initial weight (IW), and then syringe-infiltrated with an apoplast wash solution (AWS). For metabolomics analysis, a solution of



methanol/water (20:80; v/v) was used as the AWS. Assays for apoplast hydration and bacterial isolation for elemental analysis used sterile water as the AWS. Next, the surfaces of the leaves were blotted dry with a paper towel and re-weighed to acquire the after infiltration weight (AIW). Apoplast liquid and bacteria were recovered by centrifugation at 2,500 x g at 4°C for 10 min. Leaves were again weighed to obtain the after spin weight (ASW) before being flash frozen in liquid nitrogen prior to storage at -80°C. Apoplast extract, including resuspended bacteria when present, was transferred to a 1.5-mL microfuge tube and centrifuged at 2,500 x g for 5 min at 4°C to re-pellet any bacteria or cellular residue. Supernatants were placed in a fresh tube and flash frozen in liquid nitrogen. Bacterial pellets were also flash frozen prior to storage at -80°C.

Detached leaf assay

Intact plants were infiltrated by the vacuum infiltration method described above and let sit on the benchtop for 1 h. The top 5-6 cm of the first true leaves were detached by cutting with sterile scissors and the leaves were placed, cut end down, into individual wells of 6-well plates containing 2 mL of 10 mM KPO₄ at pH = 7.2 and supported by a tube rack on top of the 6-well plate. These set-ups were placed in a flat with water in the bottom and covered with a clear dome, which maintained humidity at \sim 90%. The bottom 1 cm of the detached leaves were cut off prior to apoplast extraction.

Liquid Chromatography - Tandem Mass Spectrometry (LC-MS/MS)

For LC-MS/MS analysis, frozen apoplast extracts (approximately 70 μ L each) were lyophilized and resuspended in 200 μ L of 20% aqueous methanol containing uniformly labeled 13C internal standards: 125 μM [U-13C]-glycine, 250 μM [U-13C]-glucose, 25 μM [U-13C]-fumarate, and 10 μM [U-13C]-benzoic acid. Amino acids, sugars, organic acids (OAs), and phosphorylated compounds (PCs) were obtained from dry maize leaf tissue via boiling water extraction as described in (Cocuron and Alonso, 2014; Cocuron et al., 2014). At the time of extraction, 10 μL of internal standard solution (5 mM [U-13C]-glycine, 10 mM [U-13C]-glucose, and 1 mM [U-13C]-fumarate) were added. Extracts were resuspended in 350 μL of ultrapure water, cleaned and prepared for LC-MS/ MS analyses as described in (De Souza et al., 2015). LC-MS/MS analyses of water-soluble metabolites (amino acids, sugars, PCs, and OAs) were completed according to the parameters described in (Cocuron et al., 2014).

Phenolic compounds from maize leaves were extracted as follows: 10 µL of 10 mM [U-13C]-benzoic acid internal standard and 1 mL methanol:water (40:60; v/v) solution were added to 10 mg dry leaf powdered tissue. Samples were mixed for 5 min at 30 Hz in a bead beater prior to 10 min sonication. Extracts were spun for 10 min at 14,000 x g at room temperature and supernatants were filtered with 3 kDa Amicon 0.5 Ultracel microfuge filters for 30 min at 14,000 x g at room temperature. Leaf and apoplast phenolics were analyzed according to the LC-MS/MS parameters described in (Cocuron et al., 2019).

The LC-MS/MS extract dilution and injection volumes were as follows: Apoplast at 7 HAI: amino acids (100x, 5 μL), sugars (50x, 2.5 μL), PCs and OAs (10x, 10 μL), and phenolics (5x, 10 μL). Apoplast at 12 HAI: amino acids (200x, 2 μL), sugars (50x, 10 μL), PCs and OAs (50x, 3 μL). Apoplast at 12 HAI from DMSO treated plants: amino acids (200x, 0.5 μL). Leaf extracts at 7 HAI: amino acids (80x, 5 μL), sugars (50x, 5 μL), PCs and OAs (10x, 5 μL), phenolics (2x, 10 μL). Leaf extracts at 12 HAI: amino acids (100x, 2 μL), sugars (50x, 10 μL), PCs and OAs (50x, 3 μL). Apoplast at 6 HAI (EcDS treatments): amino acids (200x, 2 μL), sugars (50x, 2 μL), PCs and OAs (50x, 2.5 μL). Leaves at 6 HAI (EcDS treatments): amino acids (200x, 2 μL), sugars (50x, 4 μL), PCs and OAs (10x, 1 μL)

LC-MS/MS analysis was performed on an Agilent UHPLC 1290 liquid chromatographer coupled to an ABSciex QTRAP 5500 mass spectrometer at the Targeted Metabolomics Laboratory at The Ohio State University, or on an Agilent 1290 Infinity II coupled to AB-Sciex QTRAP 6500+ at the BioAnalytical Facility at the University of North Texas. LC-MS/MS data processing was completed with ABSciex Analyst 1.6.1 or 1.7 software.

The quantification of each metabolite in picomoles was accomplished using i) the 13C-labeled internal standards added at the time of extraction to account for any loss of material during sample preparation; ii) commercially available external standards injected at known concentrations. The picomole metabolite values for leaf samples were converted to pmol/mg FW as follows:

where DW indicates leaf dry weight, FW is leaf fresh weight, ASW is after spin weight (leaf after apoplast extraction), and IW is leaf initial weight. The picomole metabolite quantities for apoplast samples were converted to pmol/mg leaf fresh weight as follows:

$$\frac{\frac{\textit{metabolite pmol}}{\textit{µL extract analyzed}} \times (\textit{AIW} - \textit{ASW})}{\textit{IW}}$$

where AIW indicates after infiltration weight (leaf with fully saturated apoplast), and AIW - ASW indicates total apoplast extract volume.

Confocal microscopy

Confocal microscopy was completed as described in Gentzel et al. (2019). Briefly, at designated timepoints after infiltration with bacterial inoculum or 5% DMSO, 1 cm segments of first true leaves were submerged in 100 μg/mL propidium iodide (PI, Invitrogen #P3566 diluted in ddH₂O) for 1 h on ice. Each leaf tip was mounted adaxial side up in water and sealed with a #1.5 coverslip and





nail polish. PI-stained cells were visualized with a Nikon A1+ confocal microscope (561 nm excitation/605 nm emission) with 20x objective (numerical aperture 0.75) and 1x confocal zoom. Images were acquired with Nikon NIS-Elements v4.20 software and cropped in Microsoft PowerPoint for presentation.

Maize kernel protein quantification

B73 maize seeds were planted as described above. Each day for 15 days after sowing, three plants were harvested and the kernels carefully separated from the root and shoot tissue. Kernels were then rinsed with water, wiped dry, and lyophilized for three days. Dried kernels were weighed and ground with a mortar and pestle followed by additional grinding for 5 min in a bead beater at 30 Hz. Proteins were extracted from each sample as previously described (Cocuron et al., 2014). Protein quantification of supernatants was completed with a BioRad DC Protein Assay kit according to the manufacturer instructions.

Elemental analysis

Six-day-old maize seedlings were infiltrated with *Pnss* WT at high-titer, as described above. Aliquots of inoculum were centrifuged and bacterial pellets flash frozen in liquid nitrogen. Apoplast extracts were collected at 12 HAI using sterile water as the apoplast wash fluid. Bacterial pellets were separated from the liquid supernatants and flash frozen in liquid nitrogen. Pellets from inoculum or from four apoplast extracts were then pooled into a single 5x9 mm silver foil capsule for each of three biological replicates (Costech #41067) and dried at 65°C overnight. The foil capsules were then folded closed and run on a Thermo Fisher Scientific Flash 200 elemental analyzer by soil specialists at the Carbon Management and Sequestration Center at The Ohio State University. The amount of C and N was determined based on a standard curve generated from known soil samples.

QUANTIFICATION AND STATISTICAL ANALYSIS

Statistical analysis of data across treatments and/or time-points was assessed via Student's t-test (Microsoft Excel or R (https://www.r-project.org/)) or ANOVA followed by Tukey's HSD test (R or MetaboAnalyst 4.0 (Chong et al., 2018)). Method of analysis and sample number, where n represents the total number of technical replicates across all biological replicates, are indicated in the figure legends.